Field Investigations and Numerical Studies of Groundwater Recharge through Unsaturated Sand: A Methodology Applied to Central Wisconsin

Mary W. Stoertz, Mary P. Anderson, and Kenneth R. Bradbury

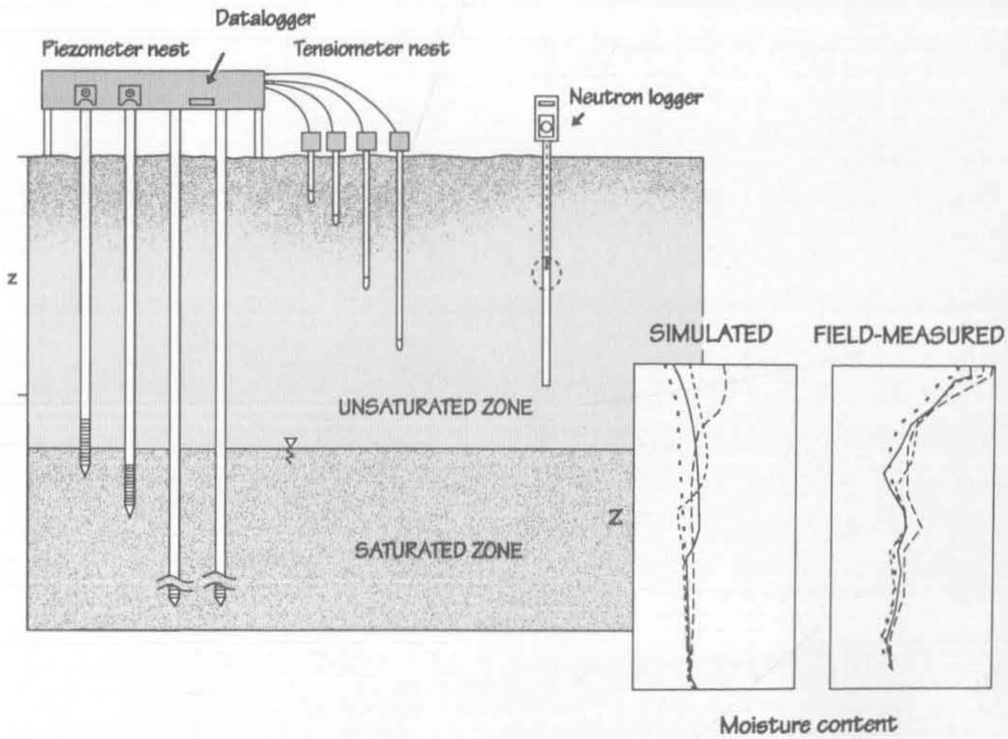

Wisconsin Geological and Natural History Survey
Information Circular 71 • 1991

Field Investigations and Numerical Studies of Groundwater Recharge through Unsaturated Sand: A Methodology Applied to Central Wisconsin

Mary W. Stoertz
Mary P. Anderson

Department of Geology and Geophysics,
University of Wisconsin–Madison

Kenneth R. Bradbury

Wisconsin Geological and Natural History Survey

Wisconsin Geological and Natural History Survey
Information Circular 71 • 1991

Published by and available from

UWEX University of Wisconsin–Extension
Geological and Natural History Survey
Ronald Hennings, Acting Director and State Geologist
3817 Mineral Point Road, Madison, Wisconsin 53705

1991

ISSN: 0512-0640

FIGURES

TABLES

Field Investigations and Numerical Studies of Groundwater Recharge through Unsaturated Sand: A Methodology Applied to Central Wisconsin

Mary W. Stoertz, Mary P. Anderson, and Kenneth R. Bradbury

ABSTRACT

To investigate controls on groundwater recharge and the variability of recharge over time, studies of recharge must include the unsaturated zone. This report presents a design for a system to monitor soil moisture, soil tension, and other parameters related to groundwater recharge through unsaturated sand in the central sand plain of Wisconsin. The calibrated model can be used to predict deep drainage, analogous to groundwater recharge, from the unsaturated zone resulting from storms of various magnitudes and intensities. Groundwater recharge in the sand plain is greatest following high-intensity, long-duration storms, but high-intensity, short-duration storms can also produce significant recharge. The monitoring system includes a design for automatic measurement and recording of soil tension at a number of points throughout the unsaturated zone using specially constructed tensiometers. We used this system to gather appropriate data for constructing soil-moisture characteristic curves determined by the instantaneous profile method. We interpreted the data with a numerical model for simulating flow through an unsaturated soil column. We calibrated the model to predict lag times between rainfall and recharge and to determine the effect of soil thickness and storm size on the timing and size of recharge pulses.

INTRODUCTION

Many hydrogeologic investigations, such as monitoring leachate movement below landfills or estimating recharge to groundwater at a site, require measurements of water movement through the unsaturated zone. The techniques and models described in this paper can be used for such investigations. In some cases, records of the water-table fluctuations or vertical hydraulic gradients in the saturated zone may suffice for quantifying recharge or leachate pulses, but in other cases direct measurements of soil moisture and tension above the water table are required. To measure recharge or deep drainage directly by tracking moisture as it moves through the soil, moisture profiles at various times are needed. For calculating recharge as a Darcian flux, the driving hydraulic gradient must be determined, usually with tensiometers. For modeling the unsaturated zone to predict moisture movement under a variety of conditions, data are needed to calibrate and test models. In particular, the functional relationship between hydraulic conductivity and moisture content is required to solve the equation for unsaturated flow.

The study described in this paper is part of a larger project to map recharge areas in Wisconsin's central sand plain and to investigate seasonal and site-specific controls on recharge. The central sand plain is an important and highly productive agricultural region that covers parts of Portage, Wood, Adams, Waushara, Juneau, Monroe, and Jackson Counties. Irrigation, heavy use of agricultural chemicals, and permeable soils have combined to make the groundwater in the sand plain susceptible to contamination by agricultural chemicals. Protecting aquifer recharge areas is one of the state regulations designed to minimize groundwater contamination. The first part of this project (Bradbury and others, in press; Stoertz and Bradbury, 1989) involved mapping aquifer recharge areas. The second part of the project, described in this paper, involved determining timing and amount of recharge at particular sites in the sand plain, focusing on the unsaturated zone. Controls on recharge were determined using an unsaturated flow model calibrated and verified with field data. Controls tested with the calibrated model include thickness of the unsaturated zone and the duration and intensity of rainfall.

Studying the unsaturated zone at a site in the sand plain required developing and testing a monitoring system for a deep, sandy soil. Many of the techniques we used were developed originally by soil scientists for use in soils less than 1 m deep. Applications of these techniques to deeper soils in the context of recharge or deep drainage are rare. We expect that our data and monitoring design will be valuable for planning future research in similar materials.

Although the project is aimed at calculating recharge rates, we did not measure recharge but deep drainage (that is, the monitoring system does not extend all the way to the water table). Deep drainage across the plane of the water table is identical to recharge.

THEORY

A basic understanding of the equations governing unsaturated flow provides the context for describing the data collection. In the first section, the governing equation (the Richards equation) is presented. The Richards equation forms the basis of the unsaturated flow model.

Governing equation

Flow through unsaturated soils is governed by an equation analogous to Darcy's law for saturated soils (Darcy, 1856), which states that the flux of water q through a cross-sectional area of an aquifer is directly proportional to the hydraulic gradient driving the flow, where the proportionality constant is the hydraulic conductivity. Thus, for one-dimensional saturated flow in the vertical direction, $q_z = -K_z(\partial h/\partial z)$, where K_z is vertical hydraulic conductivity. The hydraulic head (h) is the sum of the pressure and elevation heads: $h = h_p + z$, where h_p is positive.

For unsaturated soils, the flux q is proportional to the hydraulic gradient, but in this case the proportionality "constant" is a function of the moisture content (θ). In unsaturated soils the pressure head can be negative, arising from surface tension; hence the term *soil tension* (ψ). As before, total head is the sum of the elevation head (z) and pressure head (h_p), so $h = h_p + z = \psi + z$.

Because the pressure head is negative in the unsaturated case, ψ is intrinsically negative. When flow is essentially vertical, the form of Darcy's law that applies is written

$$q = -K(\theta)\frac{\partial h}{\partial z} = -K(\theta)[\frac{\partial \psi}{\partial z} + 1], \tag{1}$$

where the subscript on K is dropped for convenience.

To conserve fluid mass, the moisture change of a profile with time will be reflected as a change of flux with depth, or

$$\frac{\partial \theta}{\partial t} = -\frac{\partial q}{\partial z}. \tag{2}$$

In simple terms, one can imagine a small volume of soil, where more water flows into the top of the volume than flows out of the bottom. There must be a net increase in water within the volume over the time period during which the flux was measured. Combining the last two equations by substituting equation 1 into equation 2, the following differential equation describing vertical unsaturated flow through a soil column results in

$$\frac{\partial}{\partial z}[K(\theta)(\frac{\partial \psi}{\partial z} + 1)] = C(\psi)\frac{\partial \psi}{\partial t}, \tag{3}$$

where $C = \partial\theta/\partial\psi$ is defined as the specific moisture capacity. Equation 3 is the one-dimensional form of the Richards equation (Richards, 1931).

Implications of the governing equation

The difficulty of studying the unsaturated zone can be understood by referring to equation 3. Unsaturated flow studies require measuring tension (ψ) rather than positive pressure, which can be determined with a simple piezometer or standpipe. Tension is usually measured with tensiometers (or, in extremely dry soil, thermocouple psychrometers). The dependence of K on θ [the $K(\theta)$ curve] must be determined, requiring an elaborate field or laboratory test, such as the instantaneous profile method (described in the next section) in which moisture content is varied systematically and the hydraulic conductivity is derived from moisture changes. Another difficulty with unsaturated studies is determining the relationship between moisture content (θ) and tension (ψ). This functional relationship between θ and ψ is called the soil characteristic curve [$\theta(\psi)$], and is required to obtain C in equation 3. It is usually measured by laboratory tests on cores. The characteristic curve is hysteretic (Rubin, 1967; Bouma and Denning, 1974); however, we have chosen to neglect hysteresis. (We discuss the implications of neglecting hysteresis in the discussion section.)

Solving the unsaturated flow equation is considerably more complicated than solving the analogous saturated flow equation because K and C are functions of θ. Moreover, the conductivity and the moisture capacity curves are sensitive to small changes in moisture content. Instabilities may arise in the numerical solution of equation 3 as a result of this sensitivity if time steps and nodal spacing are not sufficiently small, that is, on the order of minutes and centimeters, respectively.

By solving the unsaturated flow equation, one can calculate the flux of water across the water table, or, if the water table is extremely deep, across some imaginary plane below the zone of evapotranspiration. The flux across this imaginary plane is assumed to be equivalent to groundwater recharge. Alternatively, moisture changes in a given time period throughout the column can be summed, and infiltration plus decreases in storage in the column, minus evapotranspirative losses, can be calculated as recharge. The alternative approach (but neglecting losses from evapotranspiration) is used in the model described in this paper.

Instantaneous profile method

The instantaneous profile method (Hillel and others, 1972) is a field test designed to determine the relationship between K and θ [the $K(\theta)$ curve]. We derived an equation that is the basis of the instantaneous profile method. Because the unsaturated hydraulic conductivity can be written as a flux divided by the hydraulic gradient, measurements of gradients and fluxes at different soil-moisture contents can be combined to yield the hydraulic conductivity as a function of moisture content. To determine the conductivity over a large range in the field, the soil profile must be artificially wetted to obtain high moisture contents and then allowed to drain for a long period for low moisture contents. We flooded an instrumented plot and then covered it to prevent further infiltration; over time it became quite dry. One can therefore assume that the flux at the soil surface is zero. Integrating equation 3 over the depth of interest, from the surface to depth D, the following relationship is obtained (assuming the flux at the soil surface is zero):

$$\int_0^D \frac{\partial \theta}{\partial t} dz = \int_0^D \frac{\partial}{\partial z}[K(\theta)\frac{\partial h}{\partial z}]dz = K(\theta)\frac{\partial h}{\partial z} \mid_D . \tag{4}$$

If W is the water content of the profile from the surface to an arbitrary depth D, then

$$W = \int_0^D \theta dz. \tag{5}$$

Taking the derivative of this expression with respect to time gives the left side of equation 4; that is,

$$\frac{dW}{dt} = \int_0^D \frac{\partial \theta}{\partial t} dz = K(\theta)\frac{\partial h}{\partial z} \mid_D = q_D , \tag{6}$$

where q_D refers to the flux at depth D. The final equation is a form of Darcy's law. Rearranging to show that the hydraulic conductivity can be obtained from instantaneous measures of the gradient and flux at each depth of interest yields

$$K(\theta) = \frac{q_D}{\partial h / \partial z}. \tag{7}$$

RELATED WORK

Studies of recharge focusing on the unsaturated zone can be divided into two categories. The first category, applied studies, includes calculations of recharge as a Darcian flux, or by analysis of gradients (for example, using the zero flux plane concept of Wellings, 1984), or by analysis of moisture content (that is, tracking a pulse of water). The second category, numerical modeling studies, includes more theoretical or conceptual studies in which recharge is calculated using saturated/unsaturated flow models. For the summary of laboratory and field studies (table 1), we assumed that the methodology will be the primary interest for those interested in designing similar systems; therefore, we tabulated the equipment and techniques used rather than summarized the conclusions. For the theoretical studies, on the other hand, we felt the primary interest is in the conceptual breakthroughs, and we have emphasized them in the summary.

Field and laboratory studies of recharge

Table 1 summarizes field and laboratory studies of recharge, indicating the objectives of each study and the equipment or techniques used.

Table 1. Summary of laboratory and field studies of recharge.

Laboratory studies	Devices for measuring soil tension (ψ)	Method for measuring moisture content (θ)	Method for measuring soil characteristic curve [θ (ψ)]	Method for measuring hydraulic conductivity (K)
Freeze and Banner, 1970	tensiometer	fixed	pressure plate	derived from ψ
Vauclin and others, 1979	tensiometer	gamma-ray attenuation	fit data to empirical function	$K(\theta)$ from infiltration experiments $K(\psi)$ from characteristic curves
Field studies				
Freeze and Banner, 1970	tensiometer	electrical resistance cells	pressure plate	lab curves
Enfield and others, 1973	thermocouple psychrometer	—	lab methods	derived from characteristics
Nnyamah and Black, 1977	tensiometer; dew-point hygrometer	neutron logging	pressure plate	lab curves
Ahuja and El-Swaify, 1979	tensiometer	—	lab methods	field-measured
Steenhuis and others, 1985	tensiometer	neutron logging	—	crust test; instantaneous profile method
Stephens and Knowlton, 1986	tensiometer	neutron logging	hanging column	instantaneous profile method

Table 1. *continued*

Laboratory studies	Devices for measuring soil tension (ψ)	Method for measuring moisture content (θ)	Method for measuring soil characteristic curve [θ (ψ)]	Method for measuring hydraulic conductivity (*K*)
Sophocleus and Perry, 1984-85	tensiometer	neutron logging; gypsum blocks	hanging column; pressure plate/ membrane	derived from characteristic curves
Wellings, 1984	tensiometer; resistance blocks	neutron logging	fit data to empirical function	—
Nixon and Lawless, 1960	—	neutron logging	—	—
Gee and Kirkham, 1984	—	neutron logging; lysimeters	—	—
This study	tensiometer	neutron logging	fit data to empirical function	instantaneous profile method

Laboratory studies	Material	Objective
Freeze and Banner, 1970	fine to medium sand	Measured recharge; verified numerical modeling study.
Vauclin and others, 1979	fine river sand	Measured magnitude and timing of recharge.
Field studies		
Freeze and Banner, 1970	sand, sandy loam, sandy gravel	Measured recharge; verified model; Saskatchewan, Canada.
Enfield and others, 1973	uniform sand to loamy sand	Measured water flux above a deep water table; Washington state.
Nnyamah and Black, 1977	gravelly sandy loam	Measured water flux above root zone in forest.
Ahuja and El-Swaify, 1979		Measured deep percolation below forested watershed.
Steenhuis and others, 1985	sandy soil	Measured recharge; Long Island.
Stephens and Knowlton, 1986	sand	Measured recharge; New Mexico.
Sophocleus and Perry, 1984-85	sand	Measured recharge; Kansas.
Wellings, 1984	chalk	Measured recharge using zero flux plane concept; England.
Nixon and Lawless, 1960	sand	Measured recharge by tracking moisture profiles; S. California.
Gee and Kirkham, 1984	coarse sand	Measured deep drainage; E. Washington state.
This study	sand	Measured deep drainage; Wisconsin.

Numerical modeling studies of recharge

Freeze (1969) and Freeze and Banner (1970) concluded that recharge and discharge rates are controlled by the regional flow system, but that to sustain the prevailing rates the groundwater must be replenished by infiltration in recharge areas (and implicitly, water is extracted via evapotranspiration or drainage in discharge areas). Hence, one can view recharge from two perspectives: (1) the regional flow (saturated flow) system, and (2) the unsaturated zone, which acts as either a sink or source of the water driving the regional flow system. We took the regional flow perspective in previous papers (Bradbury and others, in press; Stoertz and Bradbury, 1989). Studies taking the unsaturated zone perspective have been conducted by a number of investigators, including Pikul and others (1974) and Cichowicz (1979), who used unsaturated column models to calculate the recharge into saturated models linked to the columns. Although other researchers have used integrated rather than linked saturated/unsaturated flow models to study recharge (for example, Freeze, 1971; Winter, 1983), applications at the field scale to real field problems are rare. A field-scale example of an integrated saturated/unsaturated flow model is a study by Frind and Verge (1978), who concluded that it may not be practical to model field-scale problems with integrated models because of nodal size incompatibility between the saturated and unsaturated zones. To match the zones properly, nodes that are decimeters in size would be needed in the saturated zone. Frind and Verge (1978) suggested a return to linked models (for example, Pikul and others, 1974). The main limitations on making field-scale models are computing ability (which is becoming less of a limitation) and data availability. Because of these limitations, recharge studies tend to be restricted to single-column models of the unsaturated zone, which are used to calculate drainage (for example, this study), lag time between infiltration and recharge (for example, Watson, 1986), or water-table rise (for example, Krishnamurthi and others, 1977; Fayer and Hillel, 1982). In this context, models are more useful as conceptualizing tools than as predictive tools.

PROJECT DESCRIPTION

Purpose and procedure

Our purpose was to determine controls on the timing and quantity of water reaching the water table as recharge in response to precipitation. We installed equipment to monitor precipitation, soil moisture, and soil tension with the intent of using the data to calibrate and verify a numerical model of an unsaturated soil column (appendix A; data files in appendix B). This model could then be used to test controls on, and the timing of, recharge. The controls we investigated include the thickness of the unsaturated zone and the intensity and duration of rainfall events.

Site description

The study site (fig. 1) is about 1 km south of Wisconsin Rapids in Wood County, Wisconsin. The site is at the Griffith Nursery operated by the Wisconsin Department of Natural Resources. The instrumented area is on bare ground 8 m from the edge of a field of small pine trees. On the

Figure 1. Map of Wisconsin Rapids area showing location of the experiment site at the Griffith Tree Nursery (arrow).

north side of the field, 10 m from the study site, a double row of 15 m tall pine trees serves as a windbreak; 15 m to the west is forested land, with pine, oak, and underbrush. We did not encounter roots during drilling, so we assume that soil moisture is unaffected by transpiration. The soil surface is sandy; in an infiltration test during which 4 cm of water was ponded on the site, the infiltration rate was close to 1 m per day. The upper 30 cm of sandy soil, classified as a Plainfield Sand (Hole, 1976), is richer in fine material and organics than the soil below.

The position of the water table, 10 m below the ground surface, fluctuated less than 0.3 m during 1984. Precipitation measured at the study site in 1984 was 88 cm, occurring on 104 days, so the soil remained wetter than in average years (79 cm at Wisconsin Rapids). Because the soil is well drained (Bartelme, 1977), runoff is negligible. During the winter, surface soils are usually frozen but midwinter thaws may allow infiltration (Stoertz, 1985). The stratigraphic section consists of an upper 0.3 to 0.6 m thick, reddish-brown, medium to coarse, moderately sorted sand, with some silt (Plainfield Sand). This is underlain by 7 m of well sorted, medium to coarse sand deposited by glacial meltwater streams or deposited offshore in a glacial lake (Horicon Formation, Clayton, 1986). At 7.3 m, a silty layer about 0.5 m thick was encountered, which is believed to be common in the central and western parts of the basin (Brownell, 1986). Below this, sand is found to a depth of 19 m; the sand is underlain by a dark reddish-brown clay that is probably the weathered top of the crystalline bedrock.

Unlithified material at the site was sampled at 1.5 m intervals using a Shelby tube above the water table and disturbed auger cuttings below the water table. The Shelby tube samples were measured for volume, weighed and dried, weighed again to calculate the moisture content, packed into permeameters for saturated hydraulic conductivity determination, dried, immersed in water for porosity determination, air-dried, and finally sieved for grain-size distribution. The resulting data (table 2a; fig. 4 of Stoertz, 1985) indicated that the unconsolidated material is predominantly homogeneous well sorted sand, except for the silty layer at 7.3 m, which may have profound effects on the timing of recharge to the aquifer. Because of this silty layer, which is below the depth of monitoring, we restrict our discussion to deep drainage rather than recharge.

Porosity values (table 2a) are consistent with published values of porosities for alluvium with median grain diameters between 0.28 and 0.45 mm (Davis and DeWiest, 1966). Saturated hydraulic conductivities were determined by permeameter tests and also by an empirical equation (Masch and Denny, 1966) relating five grain-size parameters (D_{95}, D_{84}, D_{50}, D_{16}, and D_{5}) to hydraulic conductivity. The conductivity values obtained by the method of Masch and Denny are believed to be more accurate because the samples were disturbed in the process of collecting and again in packing the permeameter tube.

Table 2a. Hydraulic characteristics of samples from the study site, including saturated hydraulic conductivity determined by permeameter test and by empirical equations using grain-size distribution.

Depth (cm)	Porosity (%)	Hydraulic conductivity (cm/sec) by permeameter	Hydraulic conductivity (cm/sec) by grain size
0	44.5	0.0049	0.0070
30	36.5	0.012	0.023
150	37.1	0.014	0.014
300	39.6	0.023	0.019
460	38.5	0.016	0.023
600	40.5	0.088	0.018
730	—	—	0.003
1040	—	0.007	—
1160	—	0.004	—

Table 2b. Saturated hydraulic conductivity values (cm/sec) for the entire drainage basin as determined by various methods.

Method	Number of samples	Lower endpoint (95% confidence interval)	Upper endpoint (95% confidence interval)	Geometric mean	Standard deviation of log (K)
Aquifer pumping test	11	0.019	0.40	0.087	0.98
Specific capacity test	266	0.059	0.068	0.064	0.25
Slug test	48	0.013	0.037	0.022	0.79
Permeameter test	8	0.001	0.25	0.013	1.53
Grain-size analysis	71	0.027	0.055	0.038	0.68

METHODOLOGY

Soil tension

Principles of tensiometer operation

A clear description of tensiometer operation is Article 6 of the Soilmoisture Equipment Corporation (no date) literature, excerpted here.

> A tensiometer consists of a tube, sealed at one end by a porous ceramic cup which is in contact with the soil. The other end of the tube is above ground and is connected to a vacuum gauge [or pressure transducer]. This end of the tube is sealed after the tube has been filled completely with water.
>
> The pores in the ceramic cup are reasonably uniform and of controlled maximum size. When the porous ceramic is wetted and the pores filled with water, the surface tension of the water at the air-water interface, at each of the pores, seals the pores. Water can flow through the pores but the water film at each pore acts like a thin rubber diaphragm and will not let free air pass, throughout the working range of the tensiometer.
>
> [In damp soil] films of water are bound to each of the soil particles by strong molecular forces. As soil dries out, these water films become thinner and more tightly bound. The "tension" thus produced within these water films causes water to be sucked from the tensiometer through the pores in the ceramic cup. As water is sucked from the tensiometer by the soil, a partial vacuum is created in the tensiometer since the unit is completely sealed except for the porous cup. As more water is removed, the vacuum inside the unit becomes higher. The amount of the vacuum is registered on the vacuum dial gauge [or registered as a voltage change in the transducer]. Water is sucked from the tensiometer by the soil until such time as the vacuum created inside the tensiometer is just sufficient to overcome the suction of the soil. At this point, equilibrium is reached and water ceases to flow from the cup. The tensiometer then reads directly the amount of "soil suction."

Tensiometers manufactured by Soilmoisture Equipment Corporation were installed at the site to depths of 30, 90, 150, and 180 cm, and the vacuum gauges were read approximately weekly. In addition, four pressure-transducer tensiometers were installed to 30, 58, 122, and 178 cm. These tensiometers were read automatically every one to three hours with a Campbell Scientific CR21 datalogger.

Tensiometer construction

The tensiometers were built following the general design of tensiometers in use at the Sheffield Waste Repository in Illinois (R. Healy, verbal communication, 1983). When constructing the instruments (fig. 2), special consideration was given to the tightness of the connections and to the permeability of the materials to air. Therefore, nylon tubing was used to connect the tensiometer bodies to the transducers, and the bodies were built of thick-walled schedule-80 PVC pipe. An epoxy stable in the soil environment was purchased from Soilmoisture for attaching the ceramic cups. At PVC/PVC joints, PVC cement was used liberally. At acrylic/PVC joints, a liquid acrylic cement was used, and mechanical strength was increased by machining grooves in the PVC to hold the glue. It is obvious if the acrylic seal is not continuous because the glue is visible through the clear acrylic block.

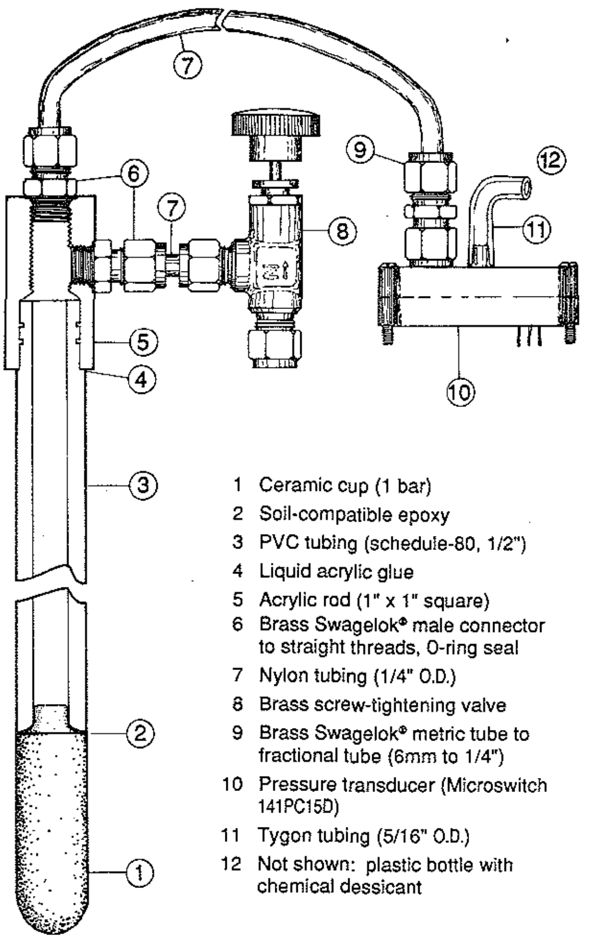

Figure 2. Diagram of a tensiometer.

The choice of fittings may ultimately determine whether a tensiometer will function, so we used machined brass Swagelok® fittings rather than less expensive plastic ones. We used O-ring seals rather than thread seals because they are better for vacuum applications, and because the acrylic block is not especially strong mechanically. It is easy with the clear acrylic block to assess the integrity of the O-ring seal.

The connection between the transducer and the nylon tubing proved to be the most difficult to seal and was the most frequent cause of tensiometer failures. A transducer with a fitting installed by the manufacturer, or a sturdier transducer housing, would be an improvement. Future researchers should try to find a better way to connect the transducer.

The transducer is a +15 psi differential transducer made by Microswitch, which is difficult to connect to the tubing. Because this transducer has 5V full output voltage and the CR21 datalogger that we used accepts signals only up to +2.5V, a voltage divider was required. Newer dataloggers accept inputs up to 6V, so this may no longer be a disadvantage. The control board design and circuitry are shown in figures 3 and 4.

The ceramic cups are standard 1-bar cups with air-entry pressures of 20 to 30 psi. Also available are 1/2-bar, 2-bar, 3-bar, and 5-bar cups, with corresponding air-entry pressures. It is important to choose appropriate cups because the greatest expected tension should be below the air-entry pressure. Choosing cups with higher air-entry pressures, however, will result in increased response times. Although sand can dry to great tensions, the 1-bar cups were satisfactory for this study.

Tensiometer installation

To eliminate air bubbles in the tensiometer, deaired water was used to fill the cup. Distilled, deionized water was boiled at room temperature for 15 minutes in a vacuum chamber in 1-liter bottles, and the bottles were filled to the top after boiling so that turbulence would not redissolve air. We filled the tensiometers with a wash bottle that had a hole drilled near the top so air would enter the bottle through the hole, not by bubbling through the deaired water. The operator placed a

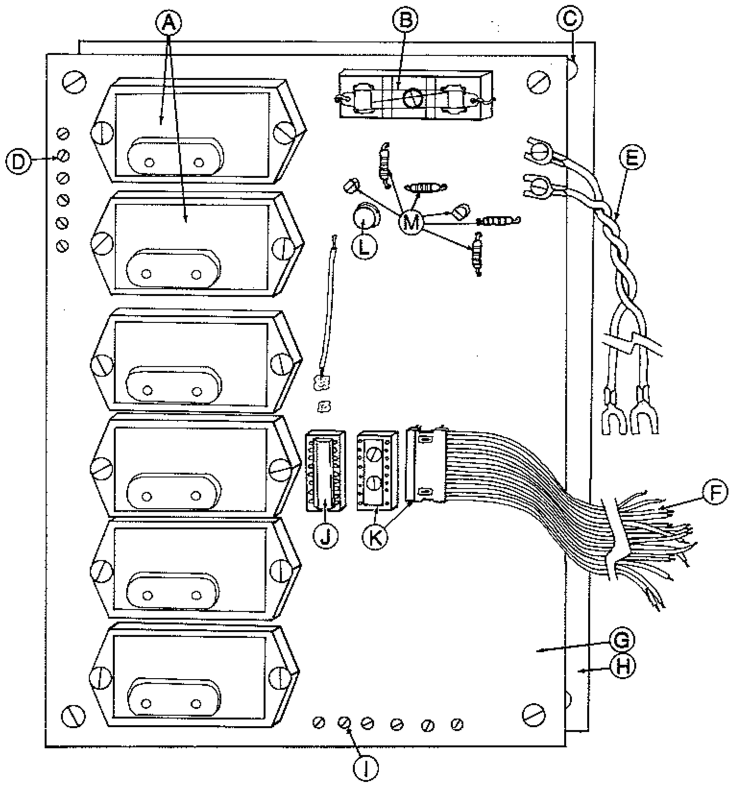

A Pressure transducers (Microswitch 141PC15D; two are spares)
B Fuse (1/4 amp)
C Spacer (1" tapped)
D Extra terminals
E To power supply (two 6V alkaline lantern batteries in series)
F Ribbon cable to datalogger
G Perforated circuit board (6" x 8" stiff unclad epoxy-glass board with larger holes drilled for bolts. Wiring is on underside.
H Protective aluminum sheet
I Terminals for other sensors
J 16-pin 3.3K resistor network for voltage divider; seated in a 16-pin socket.
K Machined 16-pin socket and ribbon-cable plug
L Voltage regulator (8V max output, 100 ma max; transducers draw 8 ma each)
M Discrete components (2N4403 transistor, 10K resistor, 5.6K resistor, 2N5172 transistor, 100K resistor, 33K resistor)

Figure 3. Diagram of tensiometer connector board.

finger over the hole while squeezing the bottle and then let air flow back into the wash bottle. Some bubbles are inevitable, precautions notwithstanding, and these bubbles are likely to cause sluggishness in tensiometer response because of the air's compressibility. We removed air periodically by flushing new water through the nylon tubing, adding it at the valve at the top of the tensiometer body while loosening the fitting at the transducer. A better system would allow air to be removed at the high point in the nylon tubing through a bleeder valve. Dissolved air might be lessened by filling the tensiometers through a small tube extending to the ceramic cup to reduce the introduction of air through turbulence as water trickles into the tensiometer.

During transport, the ceramic cups of the tensiometers were covered and cushioned to avoid clogging the pores or crushing the cups. The holes were drilled with a 2-inch Giddings soil probe to within 6 inches of the desired cup position. As the cores were withdrawn, they were dumped on a plastic dropcloth in sequence so that they could be returned to the hole in the same order, as backfill. A specially made tool, consisting of a length of galvanized 3/4-inch pipe with a sharpened, beveled end, was pushed the last 6 inches, twisted several times, and withdrawn. The tensiometer was lowered to the bottom of the hole and firmly pressed into the smaller hole. A slurry of water and excavated soil was made in a bucket using the bottom-most core, and poured down the hole. The remaining sediment was slowly sprinkled into the hole and frequently tamped with a length of pipe. There was a slight surplus of sand left after backfilling, which suggested that the material was effectively restored to its natural packing density, taking into account the volume displaced by the tensiometer itself.

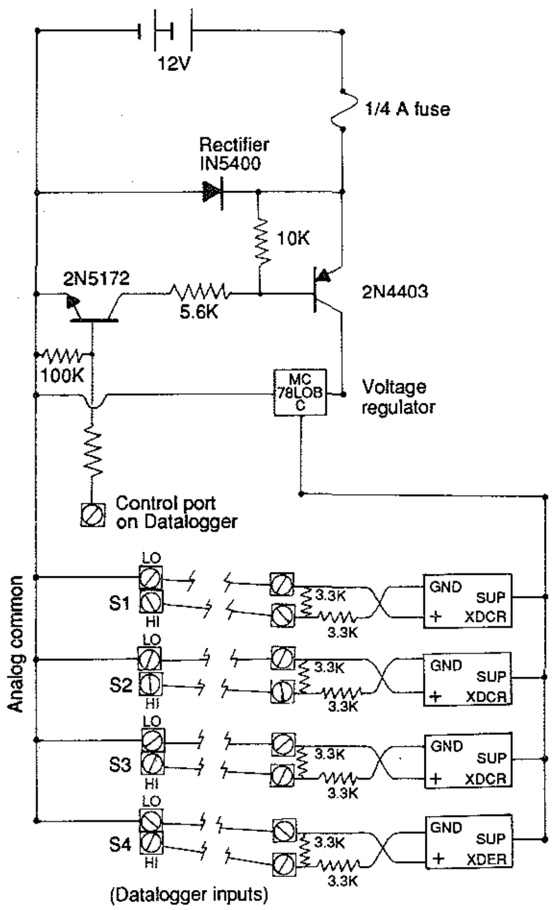

Figure 4. Circuit diagram of connector board (design by Lee Powell, University of Wisconsin-Madison, Department of Geology and Geophysics).

Tensiometer calibration

To compare readings, the transducer tensiometers were installed beside the four commercial gauge tensiometers. The transducer tensiometers were far more sensitive to moisture changes and responded more rapidly, although both sets of instruments approached comparable values after several hours. Calibration curves for the transducers were obtained from the manufacturer.

Soil-tension data

Transducer tensiometers were installed in July 1984 and, because of the danger of freezing the fluid-filled transducers, were drained in October. The commercial tensiometers were filled with an alcohol-water mixture and left in the ground through the winter. Tension in the unsaturated zone ranged from 0.2 m to 1.2 m during 1984 (fig. 9 of Stoertz, 1985). The high resolution and the rapid response time of the transducer tensiometers were needed for the instantaneous profile test because tension changed rapidly. Resolution of the commercial tensiometers was limited by the precision of the vacuum gauge and by the time required for reading each gauge. The main advantage of the transducer tensiometers was the automated reading, which permitted continuous measurements.

Soil moisture

Principles of neutron scattering

Summaries of neutron scattering are given by Schmugge and others (1980) and Wilson (1981). Neutron logging is based on the principle that high-energy, "fast" neutrons are slowed down, or thermalized, when they collide with nuclei of hydrogen atoms, which have a comparable mass. Collisions with heavier nuclei bounce the neutrons back with little momentum loss, so thermalization is accentuated in the presence of hydrogen. A detector counts the number of slow neutrons, from which the amount of hydrogen can be determined. Hydrogen may also be present in the form of organic material or hydrocarbons. Because these materials are present only in small quantities in the sandy soils of Wisconsin's sand plain, neutron thermalization is primarily due to soil moisture.

A neutron moisture probe (50 mc Am 241/Be source) was used to measure soil-moisture changes during one- or two-week intervals.

Installation of access tubes

Two thin-walled, machined-steel 2-inch access tubes were installed to a depth of 4.5 m at the site for moisture logging. The first tube was used for the actual moisture measurement, and the second tube, located slightly away from the site, was used for gravimetric calibration. (Soil was disturbed in collecting soils for gravimetric analysis; this placement of the second tube minimized disturbance at the site itself.) The tubes were installed using a 2-inch Giddings probe, so there was essentially no annular space.

Neutron logger calibration

The calibration curve used in this study was obtained from gravimetric determination of moisture content at the Hancock Experiment Station, 50 km south of the study site in the sand plain (with the same soil type as the study site, Plainfield Sand). Checks on the moisture content from a small number of gravimetric moisture content determinations using the second access tube located near the site revealed an error of about 2 percent moisture. We made a new calibration curve on the basis of limited data, not a full recalibration, which would have required a large number of soil samples spanning the expected range of moisture contents.

Rainfall

Two rain gauges were installed at the site. A standard Belfort weighing-bucket rain gauge provided a paper record of precipitation. A Sierra tipping-bucket gauge, although less accurate, was used for a digitized record of precipitation because it could be interfaced with the datalogger. The Belfort rain gauge was calibrated with measured volumes of water and installed 50 cm off the ground as recommended, in an area sheltered by a row of tall pine trees about 15 m from the gauge.

Unsaturated hydraulic conductivity

Solution of the equation governing unsaturated flow (equation 3) requires a functional relationship between hydraulic conductivity (K) and moisture content (θ). Several methods for obtaining $K(\theta)$ or $K(\psi)$ are available, the most accurate of which are probably the crust test (Bouma and others, 1974) and the instantaneous profile test (Hillel and others, 1972; Watson, 1966). Both are performed in place, so soil structure and layering remain relatively undisturbed. The crust test requires making large excavations to provide access to the soil pedons. For this reason, we chose to use the instantaneous profile test. (The theory of the instantaneous profile test is described in the section of this paper about theory; see equations 4 through 7.)

By frequent measurements of soil moisture (using a neutron logger) and tension (using tensiometers) at several depths in a soil profile during drainage, instantaneous values of the potential gradients $\partial h/\partial z$ can be obtained and cumulative fluxes q_D can be calculated from equation 6. Using equation 7, K can be found as a function of the soil-moisture content (θ). Figure 5 shows

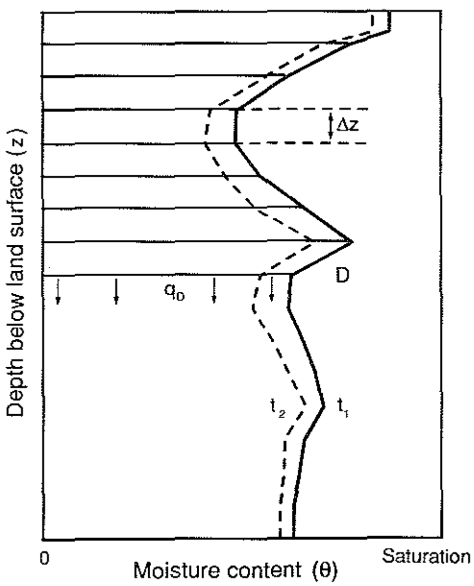

Figure 5. Schematic illustrating the calculation of the moisture flux for the instantaneous profile method. The solid line is the moisture content at time t_1; the dashed line is the moisture content at time t_2. The moisture decrease between t_1 and t_2, summed over depth increments Δz from the surface (depth = 0) to the depth D where the flux is to be calculated, is equal to the moisture flux q_D.

how the method is applied in calculating the flux that occurs between two consecutive moisture profiles, labeled t_1 and t_2. Considering a single depth increment (Δz), drainage results in a decrease in moisture content for that increment. If moisture losses ($\partial\theta/\partial t\ \Delta z$) for all such increments are measured and summed, then in absence of evapotranspiration, the moisture decrease, or change in storage for the profile, must be balanced by a flux out of the bottom of the profile. If, for example, the change in storage between t_1 and t_2 is measured for the upper 1 m of the profile (that is, D = 1 m in equation 6), that volume of water is constrained to flow across a plane at 1 m between t_1 and t_2; this flux is q. The measured θ value at 1 m is used with the flux measurement q_{1m} to calculate K for that value of θ. This procedure can be extended to calculate fluxes across planes at 1.25 m, 1.50 m, and so on. The calculated flux is defined as recharge when the plane is the water table. In this study, we calculated the deep drainage flux across a plane at 5 m below the soil surface.

Instantaneous profile method

A 2 m square area at the study site containing a neutron access tube and four tensiometers was flooded for six hours at a rate estimated at 10 to 20 cm/hr, to get as close to saturation as possible. To confine the water and permit several centimeters of ponding, a sandbox frame was placed around the plot. The plot was flooded until all the moisture levels down to a depth of 4 m had stabilized; ponded water disappeared within minutes after flooding ceased. Moisture profiles are shown in figure 6. After flooding, the plot was covered with plastic to limit evaporation and allowed to dry. Soil moisture and tension were measured hourly until changes were very small (figs. 7 and 8). The entire procedure took about 72 hours. For finer soils, several weeks might be required for drainage (Hillel and others, 1972).

By measuring the slope of the soil moisture versus time (fig. 7), $\partial\theta/\partial t$ can be obtained for different time intervals (table 3 of Stoertz, 1985). Multiplying the depth increment by the moisture change with time for that increment yields a change in moisture content or drainage. Adding the drainage for all the increments up to level D yields the flux at point D (q_D) for a given time (equation 6). The remaining unknown needed to calculate $K(\theta)$(equation 7) is $\partial h/\partial z$.

The hydraulic gradient $\partial h/\partial z$ is obtained by replotting the tension versus time curve (fig. 8) as total potential [including tension (ψ) and elevation (z) potentials] as a function of soil depth, for

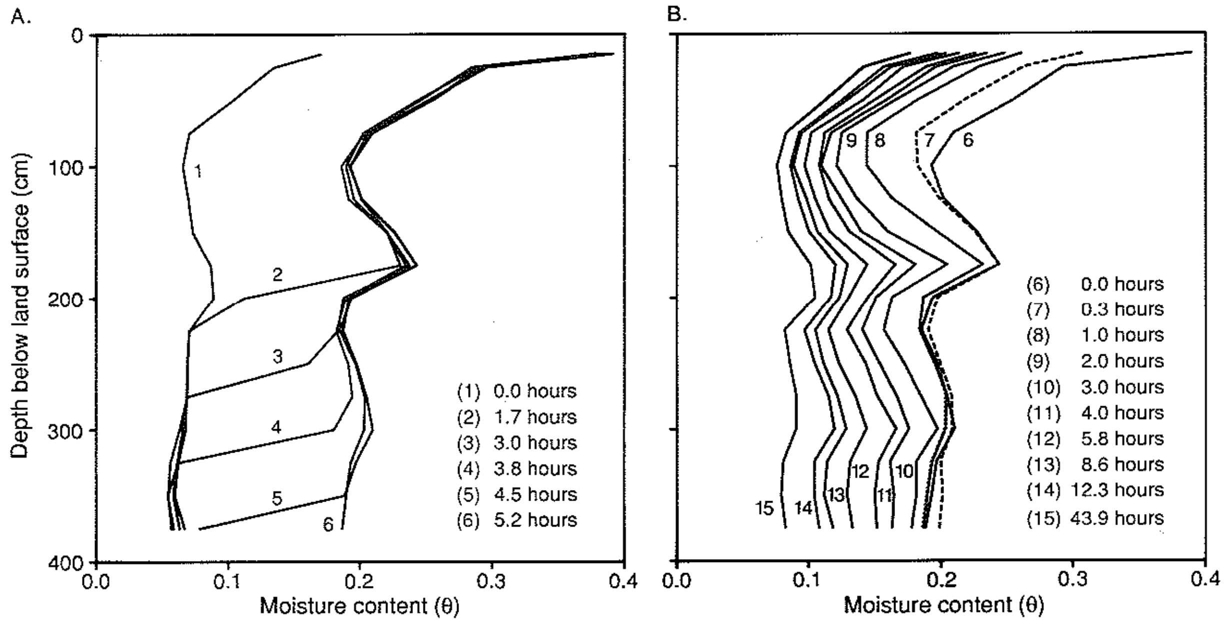

Figure 6. Field-measured soil-moisture profiles during the instantaneous profile test. **A** shows six profiles for times since flooding began; **B** shows ten profiles for times after flooding stopped and draining began.

each measurement time. Gradients are calculated from the slope of such a plot (fig. 24 and table 4 of Stoertz, 1985).

Dividing q_D by $\partial h/\partial z$ yields a value of K for the prevailing moisture content (equation 7 and fig. 9). The soil profile would be judged to be homogeneous if the entire profile could be characterized by a single curve. Instead, there appear to be at least three different types of layers in the profile. The surficial layer differs markedly from the other layers, and there also appears to be a low-conductivity layer at 1.75 m (shown in fig. 9 and in the moisture logs). The remainder of the profile consists of material with similar hydraulic properties.

Because three of the original six tensiometers failed before or during the test, complete data are available for only three depths (30, 122, and 178 cm). These data indicate a nearly linear relationship of total hydraulic head with depth. Unless the soil profile is truly homogeneous and at steady state, one would expect a nonuniform increase in tension with depth. That the profile is not homogeneous is evident in figure 9. Error introduced by using the linear relationship propagates through the calculations for hydraulic conductivity. Flux calculations, which are based solely on moisture logs, will be unaffected by errors in the head versus depth graphs, but gradient calculations may be in error.

Jones and Wagenet (1984) summarized methods of calculating $K(\theta)$ that assume a unit gradient throughout the unsaturated profile, so there is some precedent for using a linear h versus z relationship. However, more tension data are desirable to lessen the uncertainty in the profile characterization.

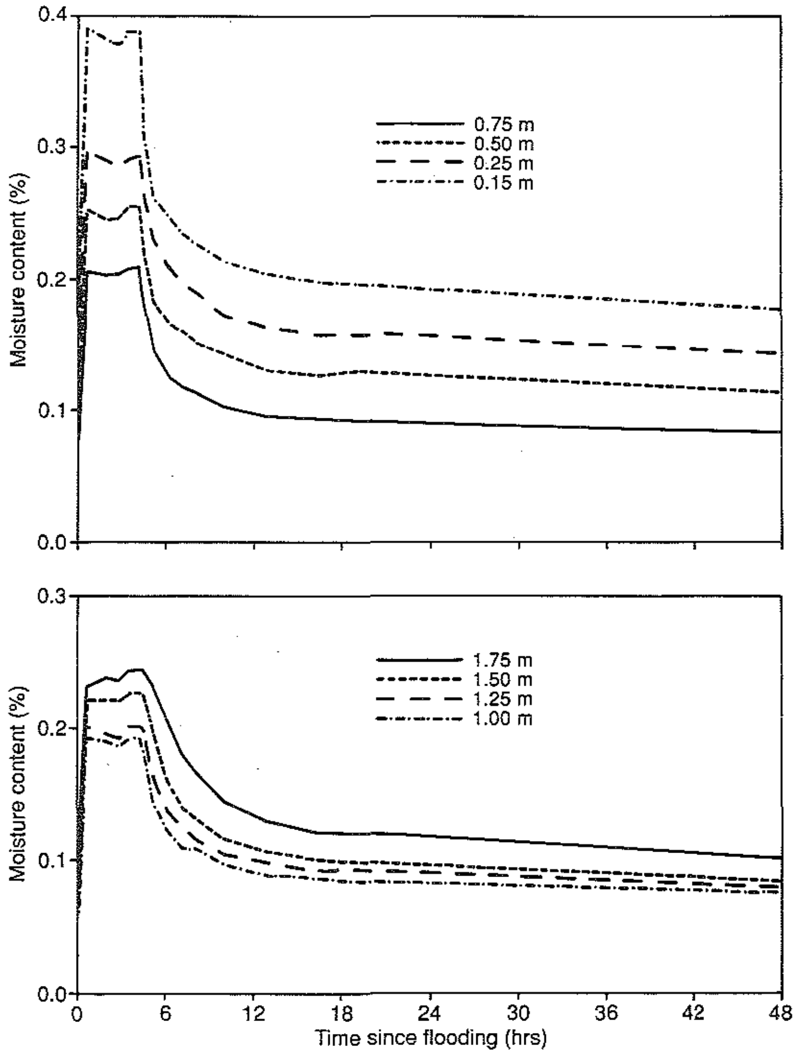

Figure 7. Field-measured soil-moisture changes with time during the instantaneous profile test. Each curve corresponds to a different depth below land surface. Times are relative to the start of flooding; time = 0 corresponds to 1:45 pm on 8/31/84.

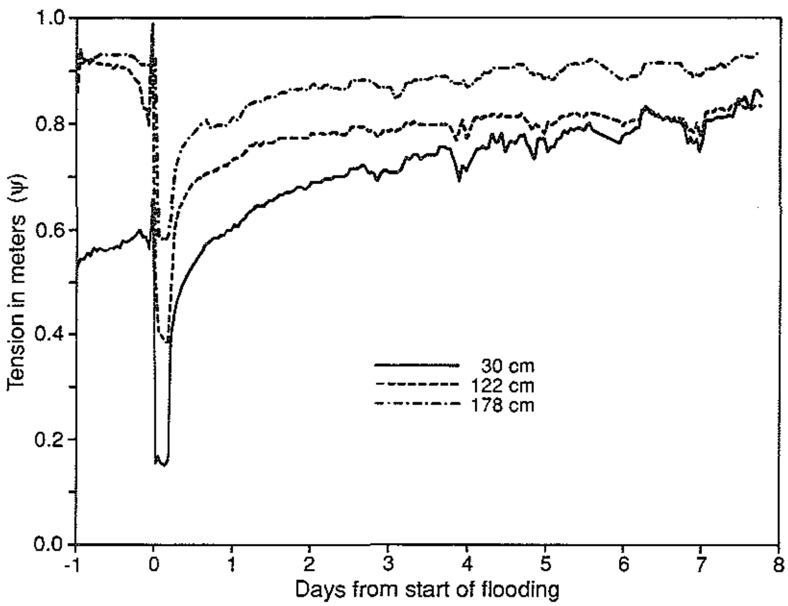

Figure 8. Field-measured soil-tension changes with time during the instantaneous profile test. Each curve corresponds to a different depth below land surface. Times are relative to the start of flooding; time = 0 corresponds to 1:45 pm on 8/31/84.

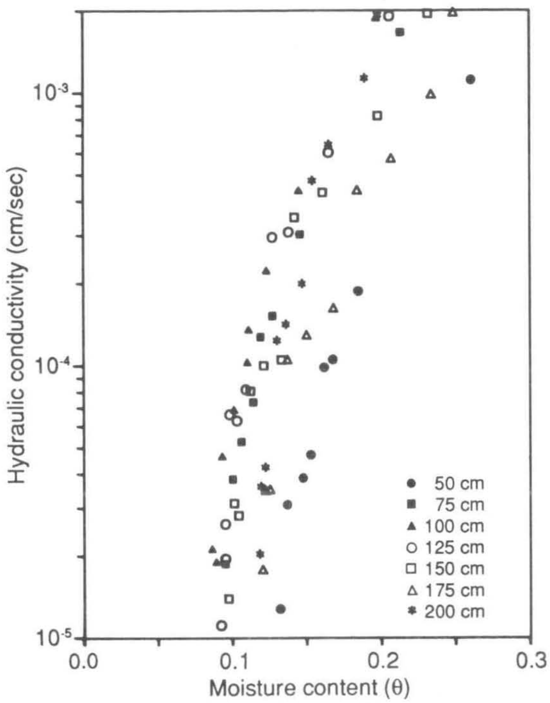

Figure 9. Hydraulic conductivity (K) versus soil-moisture content (θ) at seven depths below the land surface (50, 75, 100, 125, 150, 175, and 200 cm) determined with the instantaneous profile method.

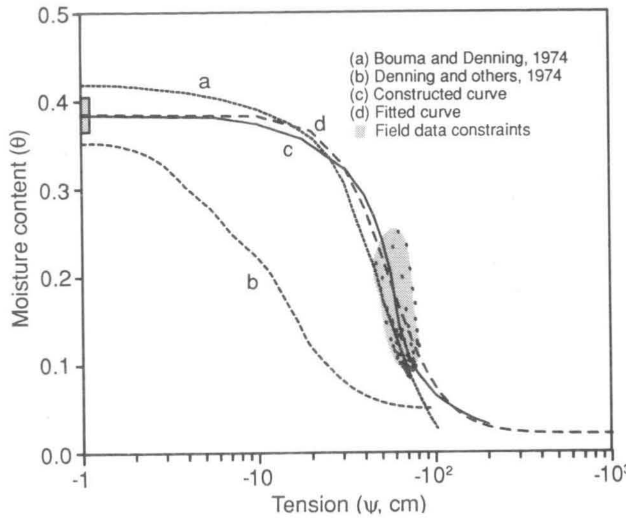

Figure 10. Soil moisture (θ) versus tension (ψ) curves. Curves a and b are draining curves for Plainfield Sand, C horizon, determined in the laboratory. Curve c is constructed from available data, showing constraints as gray areas. The large gray area contains 60 data points from the instantaneous profile test; the small gray box contains five data points from laboratory measurements of core porosity. Curve d is the best fit to curve c using Brutsaert's parameters A and B, and is the curve mathematically incorporated into the unsaturated flow model.

Calculation of the soil characteristic curve

Although it is possible in theory to obtain the soil characteristic curve [θ(ψ)] from the instantaneous profile test measurements of moisture content and tension, it may be difficult to get the full range of values. In our case, the relatively low permeability surface layer and limitations on ponding depth prevented wetting the deep (122 and 178 cm) layers beyond about 20 percent moisture. Because of rainy weather at the end of the test, the test was terminated before very dry conditions were reached. To avoid these problems, researchers often use moisture characteristics obtained in the laboratory using soil cores. A hanging column of water or a pressure plate is used to control the soil tension, and moisture content is obtained gravimetrically.

Published curves are available for some well known soils (table 3 lists curves available for sand), although they should be used with caution because the characteristic curve may vary significantly within a soil series (Denning and others, 1974; Baker, 1978). For this study, we used a combination of published curves and parts of curves obtained during the instantaneous profile test to create a characteristic curve. The section of this paper about modeling describes how the curve was incorporated into the unsaturated flow model.

Table 3. Previously published characteristic [$\theta(\psi)$] and conductivity [$K(\psi)$, $K(\theta)$] curves for sands.

Source	Soil type	Curve calculated $\theta(\psi)$	$K(\psi)$	$K(\theta)$
Baker, 1978	Plainfield Sand		x	
Bouma and Denning, 1974	Plainfield Sand, C	x		x
Brooks and Corey, 1964	Hygiene Sandstone	x	x	
Brooks and Corey, 1964	Loveland fine sand	x	x	x
Denning and others, 1974	Plainfield Sand, B2,C	x	x	x
Freeze and Banner, 1970	Meota Sand	x		
Freeze and Banner, 1970	Yorkton sandy loam	x		
Freeze and Banner, 1970	Whitesand Sandy Gravel	x		
Freyberg and others, 1980	Monterey Sand		x	
Gee and Kirkham, 1984	coarse sand			x
Hillel and others, 1972	alluvial sandy loam			x
Kovacs, 1986	Columbia sandy loam	x		
King, 1965	G.E. no. 2 sand	x	x	
Nnyamah and Black, 1977	Dashwood gravelly sandy loam	x	x	x
Reeder and others, 1980	well-graded Monterey dune sand	x		x
Rubin, 1966, 1967	Rehovot Sand	x	x	
Steenhuis and others, 1985	Haven Loam (outwash)		x	
Stephens and others, 1986	fine alluvial sand	x	x	x
Stoertz, 1985	Plainfield Sand		x	
Topp, 1969	Rubicon sandy loam	x		x
Vauclin and others, 1979	fine river sand	x	x	

Figure 10 shows two published characteristic curves for Plainfield Sand. Curves a (Bouma and Denning, 1974) and b (Denning and others, 1974) are draining curves for pure Plainfield Sand, C horizon, obtained with standard laboratory procedures (Richards, 1965). Curve c is the constructed curve based on field data from the study site; 60 data points (shown as a gray area in fig. 10) were obtained from the instantaneous profile test. Other data used to complete curve c were measurements of the saturated moisture content (porosity), which vary from 36.5 to 40.5 percent (table 2a, and shown as a gray box in fig. 10), except for the surface layer, which has a porosity of 44.5 percent. We assumed a saturated moisture content of 38.5 percent, which also falls between the values from curves a and b. The error that can arise from using our constructed curve is probably as much as 7 percent moisture content. Without the constraining values from the instantaneous profile test, the possible error from using curves a and b is as much as 25 percent moisture content.

MODELING

Purpose

We developed a one-dimensional numerical model (appendix A) to simulate flow in a column of unsaturated soil. Unsaturated models are useful as tools for studying controls on unsaturated flow and drainage or groundwater recharge. If properly calibrated and verified, such models can also be used for predicting moisture and tension distributions in a soil column or drainage (groundwater recharge) from a column, in response to a given amount of infiltration.

Model description

The governing equation for one-dimensional unsaturated flow is equation 3. The model (fig. 11) simulates a vertical soil column and consists of nodes numbered upward from the water table and with a spacing of Δz. The node above the water table (M1) is numbered 2 because the model automatically places the first node at M1-1, which is a distance of Δz below M1 (in this case, at the water table). The node at the top of the column (MM) is at the bare soil surface. Because there is no provision in the model for a movable lower boundary due to fluctuations in the height of the water table, an average length for the soil column must be estimated on the basis of the length of the unsaturated zone before and after infiltration.

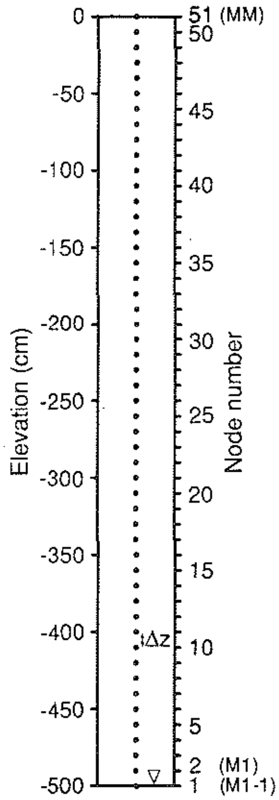

Figure 11. Schematic of the soil column used in the unsaturated model. Elevations are with respect to the ground surface (0 cm); the water table is indicated by the upside-down triangle at -500 cm. Nodes 1, 2, and 51 are designated by M1-1, M1, and MM in the model. Nodal spacing Δz is 10 cm.

The spacing between nodes (Δz) was 10 cm for this study. In unsaturated modeling the nodal spacing is usually centimeters to decimeters (Frind and Verge, 1978). Rapidly varying upper boundary conditions caused by changing infiltration rates and a steep moisture capacity ($\partial\theta/\partial z$) curve representing soil-moisture storage require that the nodal spacing be small to avoid stability problems. The time increment (Δt) must also be small, for the same reasons. We used time steps from one second to one hour. The shorter time steps are needed for simulations of high infiltration rates. Model results were printed at desired intervals, usually hourly.

The upper boundary condition at the ground surface is

$$\partial\psi/\partial z = R(t)/K(\psi) - 1, \tag{8}$$

where $R(t)$ is the net infiltration rate or rainfall intensity (positive) or evaporation rate (negative). The infiltration rate is changed in a stepwise fashion at desired time steps, to correspond to rainfall duration. The lower boundary at the water table is constrained by these conditions: $K = K_{SAT}$, $\theta = \theta_{SAT}$, and $\psi = 0$. Initial conditions are specified as tensions for each node, generally based on field conditions, which we discuss later.

Incorporating unsaturated soil curves into the model

Three unsaturated soil curves must be incorporated into the model, including the moisture characteristic $\theta(\psi)$ (to convert tension to moisture content for output), the conductivity-tension curve, $K(\psi)$, and the moisture capacity curve (C). These curves can be entered several ways—as tables of values, as line segments, and as functions using empirical equations with fitting parameters. We used the latter method in this model, using the empirical equation suggested by Brutsaert (1966):

$$\theta(\psi) = (\theta_0 - \theta_r)\frac{A}{[A + (-\psi)^B]} + \theta_r, \tag{9}$$

where θ_0 = soil-moisture content at saturation, θ_r = the "residual" θ when ψ has a very large negative value, and A and B are parameters to be fitted depending on the soil.

The advantage of Brutsaert's equation is that the same parameters A and B (plus a third parameter N) appear in an equation relating K and ψ:

$$K(\psi) = K_{sat}\left[\frac{A}{A + (-\psi)^B}\right]^N, \tag{10}$$

where N is a fitting parameter that depends on the soil type. Note that hysteresis is ignored. Determination of parameters A, B, and N is discussed in appendix C.

Because the moisture capacity (C) is defined as $\partial\theta/\partial\psi$, equation 9 can be differentiated to get C:

$$C = \frac{(\theta_0 - \theta_r)AB(-\psi)^{(B-1)}}{[A + (-\psi)^B]^2}. \tag{11}$$

Solution

Equation 3 is approximated and solved using the predictor-corrector technique of Douglas and Jones (1963) following Pikul (1973). The predictor (written for the time step from n to n +1/2) is

$$\frac{1}{\frac{1}{2}(z_{j+1} - z_{j-1})}\left[K^n_{j+\frac{1}{2}}\left(\frac{\psi_{j+1}^{n+\frac{1}{2}} - \psi_j^{n+\frac{1}{2}}}{z_{j+1} - z_j} + 1\right) - K^n_{j-\frac{1}{2}}\left(\frac{\psi_j^{n+\frac{1}{2}} - \psi_{j-1}^{n+\frac{1}{2}}}{z_j - z_{j-1}} + 1\right)\right] = C_j^n\left(\frac{\psi_j^{n+\frac{1}{2}} - \psi_j^n}{\Delta t/2}\right), \tag{12}$$

where j is the vertical space index;

$$K_{j+\frac{1}{2}} = \frac{2K_{j+1}K_j}{K_{j+1} + K_j};$$
$$K_{j-\frac{1}{2}} = \frac{2K_{j-1}K_j}{K_{j-1} + K_j}.$$

Suitable arrangement of equation 12 yields

$$A_j \psi_{j-1}^{n+\frac{1}{2}} + B_j \psi_j^{n+\frac{1}{2}} + C_j \psi_{j+1}^{n+\frac{1}{2}} = RHS_j, \tag{13}$$

where A_j, B_j, C_j, and RHS_j are entries in the coefficient matrix. A set of linear equations generated by equation 13 can be solved using the Thomas Algorithm to obtain the ψ distribution at time $n+1/2$ from which K and C at time $n+1/2$ can be calculated.

The corrector (written for the time step n to $n+1$) is

$$\frac{1}{(z_{j+1}-z_{j-1})}\left[K_{j+\frac{1}{2}}^{n+\frac{1}{2}}\left(\frac{\psi_{j+1}^{n+1}-\psi_j^{n+1}}{z_{j+1}-z_j}+1\right)-K_{j-\frac{1}{2}}^{n+\frac{1}{2}}\left(\frac{\psi_j^{n+1}-\psi_{j-1}^{n+1}}{z_j-z_{j-1}}+1\right)\right]$$

$$+\frac{1}{(z_{j+1}-z_{j-1})}\left[K_{j+\frac{1}{2}}^{n}\left(\frac{\psi_{j+1}^{n}-\psi_j^{n}}{z_{j+1}-z_j}+1\right)-K_{j-\frac{1}{2}}^{n}\left(\frac{\psi_j^{n}-\psi_{j-1}^{n}}{z_j-z_{j-1}}+1\right)\right] \tag{14}$$

$$=C_j^{n+\frac{1}{2}}\left(\frac{\psi_j^{n+1}-\psi_j^{n}}{\Delta t}\right).$$

Rearrangement of equation 14 yields

$$A_j \psi_{j-1}^{n+1} + B_j \psi_j^{n+1} + C_j \psi_{j+1}^{n+1} = RHS_j. \tag{15}$$

Equation 15 can be solved in the same way as equation 13 to obtain the ψ distribution at the new time step $n+1$.

At the upper boundary node equation 8 is rewritten in finite-difference form and directly substituted into equations 13 and 15. By repeatedly solving equations 13 and 15 for each time step, the tension at each node in the soil column can be simulated over a desired period of time. Using the equation for the soil characteristic (equation 9), tension is converted to moisture content.

Calibration to wetting and draining profiles

To calibrate the model, we simulated approximately the conditions of the instantaneous profile test and checked to see whether or not the model was able to reproduce the observed moisture profiles during the wetting and draining phases. The actual field system being modeled consists of approximately 10 m of unsaturated sand above the water table; the upper soil boundary consists of somewhat finer sandy soil. Tension and moisture data are available for only the upper 5 m, so this is the region on which we focused. For convenience, we modeled only the upper 5 m, artificially placing a water-table type boundary 5 m below the surface. This artificial boundary results in unrealistically high water contents in the lower nodes and interpretation of the flux through the 5 m plane as recharge. Thus, the moisture contents in the lower nodes cannot be compared with the field data, and the recharge flux must be considered deep drainage.

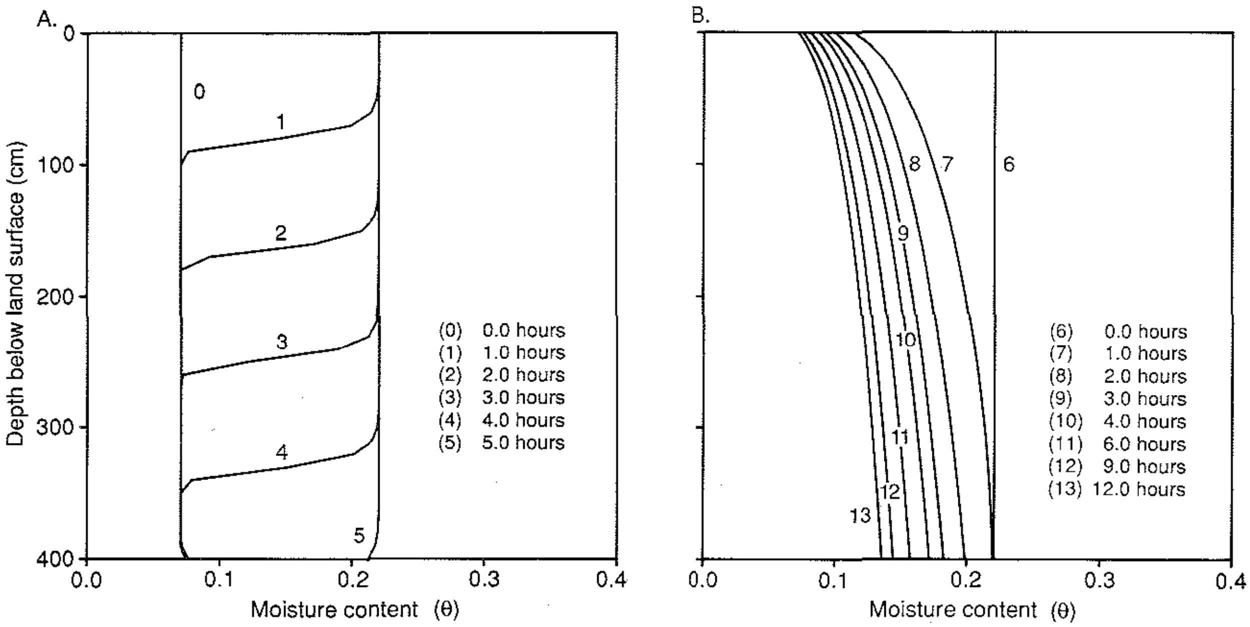

Figure 12. A: Simulated moisture profiles during flooding. Times are since start of flooding. The model was calibrated by adjusting the saturated hydraulic conductivity (K_{SAT}), infiltration rate (R), and Brutsaert's parameter N to fit these curves to the field-measured profiles in figure 6A. Parameters used here are K_{SAT} = 0.07 cm/sec, R = 0.0035 cm/sec, and N = 5. **B:** Simulated moisture profiles during draining (compare with field-measured profiles in fig. 6B). Times are since flooding stopped and draining started. Parameters are as in figure 12A except that R = 0 cm/sec.

Rather than attempting to simulate ponding over the low-conductivity surface layer, we assumed a constant flow boundary at the surface, using the conductivity for the lower part of the profile as the surface conductivity. Because we assumed a homogeneous profile even though the profile is layered, we did not expect the match between observed and simulated moisture contents, especially at the surface, to be perfect.

Initial moisture profiles (curve 1 in fig. 6A) were simulated by first calculating the infiltration rate needed to generate the profile. For example, an 8.6 percent moisture content corresponds to a -91.2 cm tension, based on the characteristic curve (fig. 10). In turn, this tension corresponds to a hydraulic conductivity of 7.9×10^{-6} cm/sec (appendix C, fig. C2), which, under an assumed unit hydraulic gradient, corresponds to an infiltration rate of 7.9×10^{-6} cm/sec. Imposing this flow rate on the upper boundary generates the steady-state 0-hr profile in figure 12. At the start of the simulation, the infiltration rate was escalated to 0.003 cm/sec, as determined from the steady-state "fully wetted" profile (curve 6 in fig. 6A).

Parameters adjusted in calibration were the saturated hydraulic conductivity, K_{SAT}, the infiltration rate R, and the curve-fitting parameter, N. These parameters were adjusted within a range of probable values. The calibrated model used K_{SAT} = 0.07 cm/sec, R = 0.0035 cm/sec, and N = 5. Discussion of choosing these values is given in the next section on sensitivity. Using the calibrated values of K_{SAT}, R, and N, measured field moisture profiles (fig. 6A) and simulated profiles (fig. 12A) indicate that the model reproduces the advance of the wetting front fairly well. The simulated draining profiles (fig. 12B) also resemble the measured draining profiles (curves 6 to 15 in fig. 6B).

Mass balance check

The mass balance can be checked for the first four hours of the instantaneous profile test when drainage is essentially zero, before the wetting front reaches the capillary fringe. At those times the infiltration should be balanced by storage changes. (The two values are printed out by the model as TR and TSTOR.) For the first four hours, infiltration and storage changes differ by approximately 0.1 percent.

After the first four hours, the mass balance can be checked manually (this step is not built into the model) by comparing the drainage calculated by the model against an independent calculation of outflow. The drainage calculated by the model is the sum of inflow (infiltration) and change in storage within the soil column for a given time period. Using equation 1, outflow from the column (drainage) can be calculated as the flux across the water table. The mass balance equation states that inflow plus change in storage equals outflow.

The tension gradient in equation 1 was calculated by averaging tension gradients above and below node 2 (that is, -490 cm); the hydraulic conductivity at node 2 was used. The mass-balance error is expressed as the absolute difference between inflow plus change in storage and outflow calculated as a flux, divided by the smaller of the two terms on either side of the mass-balance equation. The error can be greater than 100 percent in the first 36 minutes of the instantaneous profile test because the absolute difference between rates is small for early times, on the order of 10^{-6} cm/sec (compared with that of drainage rates for later times, which are on the order of 10^{-3} cm/sec). An absolute difference of 1.5×10^{-4} cm/sec or an error of 60 percent occurs at the moment the pulse from the test reaches the water table. However, the absolute difference is small relative to the drainage rates encountered in the test. After four hours, the error is less than 2 percent.

Sensitivity of the calibrated model

Calibration of an unsaturated flow model requires adjusting parameters K_{SAT}, R, and N within probable ranges until an observed field profile is matched satisfactorily. Saturated hydraulic conductivity measurements for the sand plain are tabulated in table 2b. The scale of the instantaneous profile test (several meters square) suggests that field rather than laboratory methods for determining the operational hydraulic conductivity are appropriate (Bradbury and Muldoon, 1990). Therefore, an appropriate K_{SAT} is expected to fall between 0.02 and 0.09 cm/sec. The infiltration rate (R) is determined by the water application rate during the instantaneous profile test, which varied between 0.006 and 0.007 cm/sec. Some of the water is expected to have flowed horizontally out of the column, reducing the effective infiltration rate. A probable range of R is therefore from 0.002 to 0.006 cm/sec. Values of parameter N of 5 or 6 fit the data in figure C2 reasonably well.

We calibrated the model to the field-measured wetting depth (fig. 13, dashed line) and to the average moisture content attained in the fully wetted field profile (about 0.22). In general, independently increasing K_{SAT} increases the depth of moisture penetration and decreases the moisture content. Increasing R increases the depth of wetting and also increases the moisture content at all depths. Increasing N decreases the depth of wetting and increases the moisture content. Several combinations of these parameters are shown in figure 13, including the final choice for the calibrated model (solid triangles, with legend in bold).

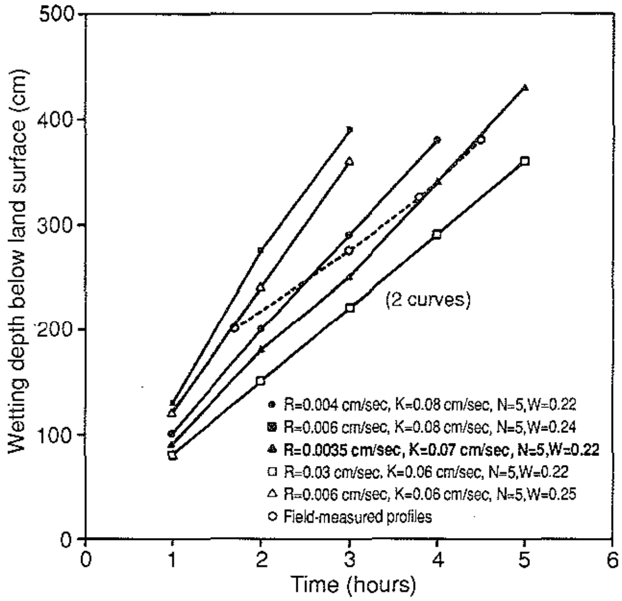

Figure 13. Sensitivity of simulated depth of wetting at different times to combined parameters R (infiltration rate), K_{SAT} (saturated hydraulic conductivity), and N (Brutsaert's fitting parameter). The primary criterion for selecting parameters in the model calibration is a match to the field-measured wetting depths (dashed line). Another criterion is a match to the steady-state moisture content (W) attained in the upper profile.

Verification with several moisture logs

It is clear from the discussion of the calibration that the final choice of parameters is not unique. For this reason, the calibrated model should be verified. We verified the model by attempting to reproduce four moisture profiles measured during the period 9/27/84 to 10/16/84. This period was chosen primarily because it was cool and rainy, justifying neglecting evaporation as an influence on the moisture profiles. Transpiration from plants is negligible because the site is bare sand, but in general, evapotranspiration is not negligible and must be subtracted from the calculated recharge flux.

Precipitation for the period 8/29/84 to 10/18/84 is described in table 4. We assumed that each storm occurs uniformly during the given time interval. Total rainfall was divided by storm duration to determine average intensity. Because the soil is very permeable, all the rainfall is assumed to soak into the ground as infiltration.

Moisture content during the period 8/27/84 to 10/18/84 was simulated using relatively dry initial conditions. Experimenting with the model indicates that even if the initial tensions are wrong, the storms between 8/29/84 (the start of the simulation) and 9/27/84 (day 30, the date of the first moisture log used for verification) overwhelmed any errors in the initial conditions.

The time step was one hour. Results were printed daily at midnight. Rainfall was turned on and off by resetting R at time steps specified in the data file (appendix B, data file B). Parameters K_{SAT}, A, B, and N were unchanged from the calibrated model.

Fifty-one daily moisture profiles were generated using data file B (appendix B). Profiles for days 15 to 19 are plotted conventionally in figure 14; the 51 profiles are stacked in a three-dimen-

Table 4. Precipitation for the period 8/29/84 to 10/18/84 used in the 51-day fall-rainstorms simulation (appendix B, data file B). The time interval is days.

Date	Time interval (from 0 hrs, 8/29/84)	Total rainfall (cm)	Rainfall rate (cm/hr)	Rainfall rate (cm/sec)	Rainfall duration (hours)
8/29/84	0.75-0.79	1.25	1.25	3.5×10^{-4}	1
9/2/84	4.25-4.33	0.25	0.13	3.6×10^{-5}	2
9/6/84	8.79-8.83	0.25	0.25	6.9×10^{-5}	1
9/8/84	10.25-10.33	0.25	0.13	3.6×10^{-5}	2
9/9/84	11.88-11.92	0.50	0.50	1.4×10^{-4}	1
9/10/84	12.83-12.92	0.25	0.13	3.6×10^{-5}	2
9/12/84	14.58-15.00	5.00	0.50	1.4×10^{-4}	10
9/14/84	16.46-16.67	0.50	0.10	2.8×10^{-5}	5
9/24/84	26.04-27.00	3.25	0.14	3.9×10^{-5}	23
9/28/84	30.13-30.38	0.25	0.04	1.1×10^{-5}	6
10/7/84	39.00-39.92	4.25	0.19	5.3×10^{-5}	22
10/12/84	44.21-44.92	2.25	0.13	3.6×10^{-5}	17
10/15/84	47.38-47.75	1.75	0.19	5.3×10^{-5}	9
10/16/84	48.50-49.00	2.50	0.21	5.8×10^{-5}	12
10/18/84	50.63-51.00	3.00	0.33	9.2×10^{-5}	9

Figure 14. Simulated soil-moisture profiles for days 15 to 19, plotted conventionally. This figure is intended to make figure 15 easier to read; note the stacked profiles for days 15 to 19 in figure 15.

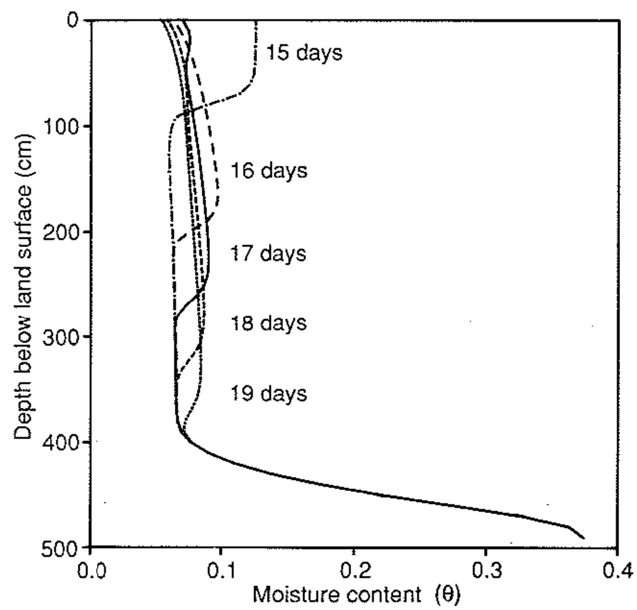

sional plot in figure 15. Movement of a recharge pulse from the soil surface to the water table is clearly visible, and there is a lag of between one and two weeks from a rainfall spike (see numbered storms) to the resulting recharge peak (see arrows in fig. 15), depending on the duration and intensity of the storm. A graph of recharge (or deep drainage) versus time, calculated by the model, is shown at the foot of figure 15.

Four simulated moisture profiles and the corresponding four field-measured profiles are shown in figure 16. The simulated and field-measured profiles in figure 16 are difficult to compare because the model assumes a homogeneous soil column; the same soil curves are used for all depths. In particular, fine layers at the surface and at about 175 cm depth were ignored. Instead of

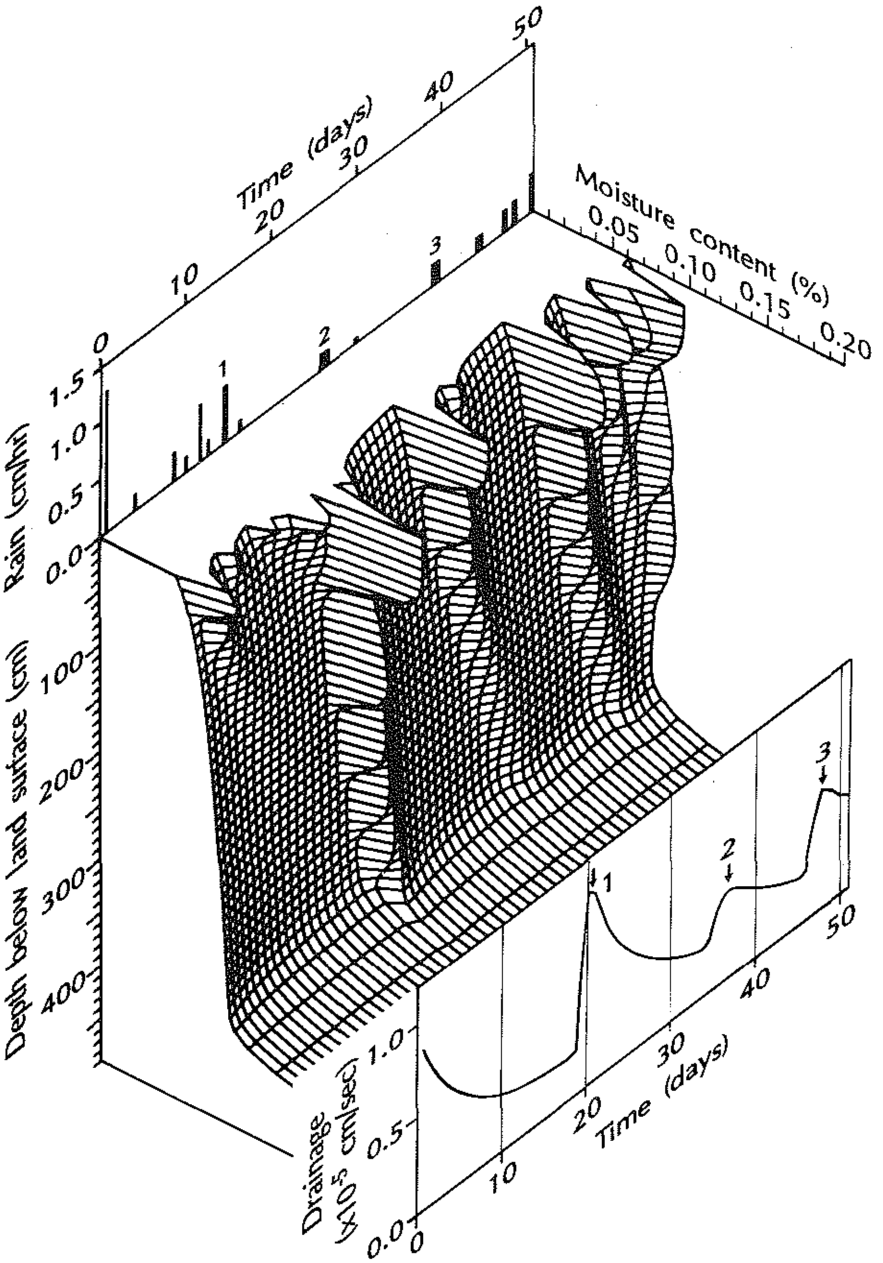

Figure 15. Three-dimensional plot of simulated soil-moisture profiles for the entire simulation period, days 0 to 51. The vertical axis is elevation, where 0 is the land surface. The time axis goes into the page. Peaks in the "topography" correspond to wet soil conditions; valleys correspond to dry conditions. The plot has been truncated at 20 percent moisture content, in effect removing part of the capillary fringe: the moisture content increases linearly to 38.5 percent at the water table (depth = 500 cm). Rainfall is shown as a bar graph at the top of the plot, using the same time scale. Drainage is shown at the foot of the plot.

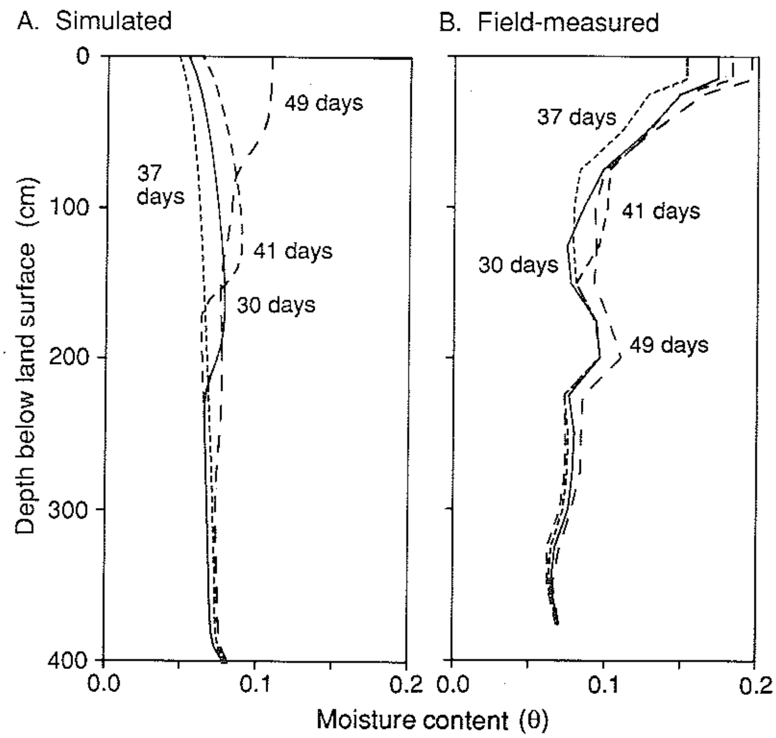

Figure 16. Simulated (**A**) and field-measured (**B**) soil-moisture profiles for days 9/27/84 (day 30), 10/4/84 (day 37), 10/9/84 (day 41), and 10/16/84 (day 49).

comparing absolute moisture contents, it is easier to compare moisture changes between successive profiles. Moisture changes are shown in figure 17 for the three intervals (A) 9/27/84 to 10/4/84, (B) 10/4/84 to 10/9/84, and (C) 10/9/84 to 10/16/84. The match in figure 17A is not especially good: downward movement of moisture has been retarded in the field profile relative to the simulated profile. This disparity may be attributed to the retarding effect of the fine surface layer and the fine layer at 175 cm, which were not incorporated into the model. Figures 17B and C show better agreement between field and simulated profiles.

Another check on the model's performance is a comparison of approximate moisture contents (figs. 16A and B) for the simulated and observed cases. The simulated profiles vary in moisture content between 6.5 and 9.5 percent, and the observed profiles vary between 6.5 and 10 percent (neglecting the fine layers at the surface and 175 cm). Thus, the model is able to reproduce the approximate range of moisture content as well as changes in moisture content. Because the calibrated model is able to reproduce the moisture logs for drier conditions reasonably well, the model is considered verified.

Water-table response to recharge

A properly calibrated model should be able to predict water-table rises resulting from recharge (that is, from drainage across the plane of the water table). A silty layer above the water table but below the unsaturated zone precluded correlating plots of water level versus time for the study site

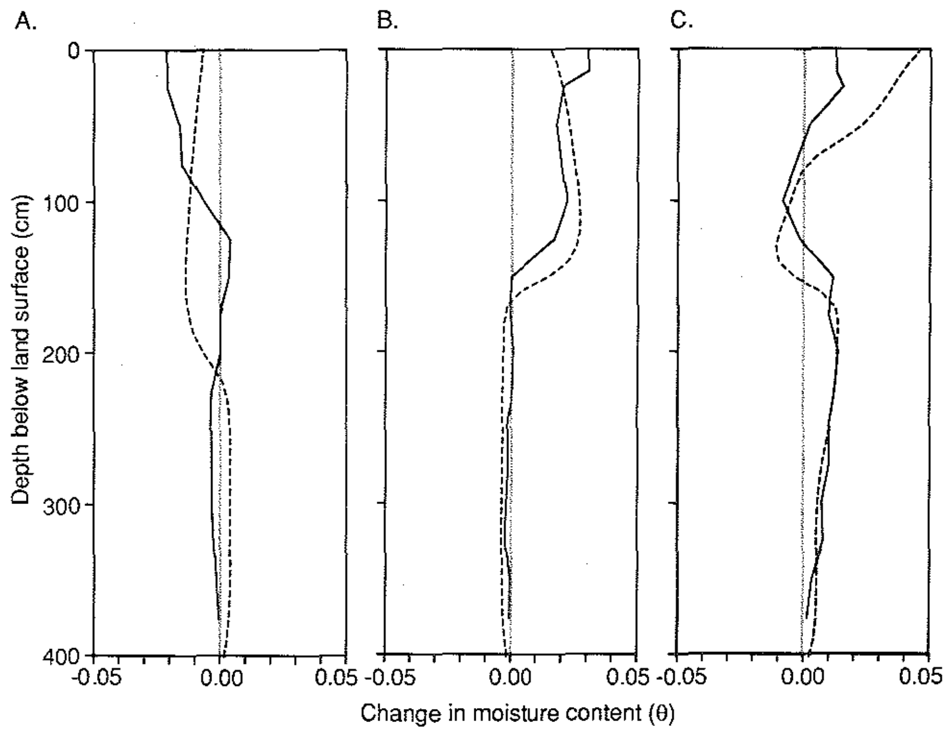

Figure 17. Changes in moisture content between successive profiles for field-measured (solid lines) and simulated (dashed lines) profiles for three intervals: 9/27/84 to 10/4/84 (**A**), 10/4/84 to 10/9/84 (**B**), and 10/9/84 to 10/16/84(**C**). Changes are determined by subtracting the moisture content at the earlier time from the moisture content at the later time; a negative change indicates an increase in moisture during the interval.

(site 1) with plots of modeled drainage versus time. A water-level hydrograph is available for a nearby site (site 2) with no silt layer (CHIK-1, Stoertz, 1985). Vertical hydraulic gradients at sites 1 and 2 are small, so water-level fluctuations in piezometers at both sites are representative of water-table fluctuations.

Model simulations of water-table fluctuations at site 2 required several simplifying assumptions.

- The depth to water at site 2 is 210 cm, so the model column must be set at 210 cm. A column length of 500 cm was used in the calibration and verification simulations described in previous sections for site 1.
- The characteristic curves were derived from data measured at site 1 rather than site 2, but the soils are similar except that there is more organic material in the upper 30 cm of site 2.
- Converting recharge (R) to an equivalent water-table rise required dividing R by S_y, where S_y is the specific yield. S_y is assumed to equal porosity, which is equal to saturated moisture content θ_{SAT}. For sites 1 and 2, we assumed that $S_y = 0.2$.

The water table at site 2 declines between recharge episodes as water enters into the regional flow system. The water-table declines can be simulated by the model by assuming (1) that the water level on any given day is an expression of the cumulative effect of all previous days of

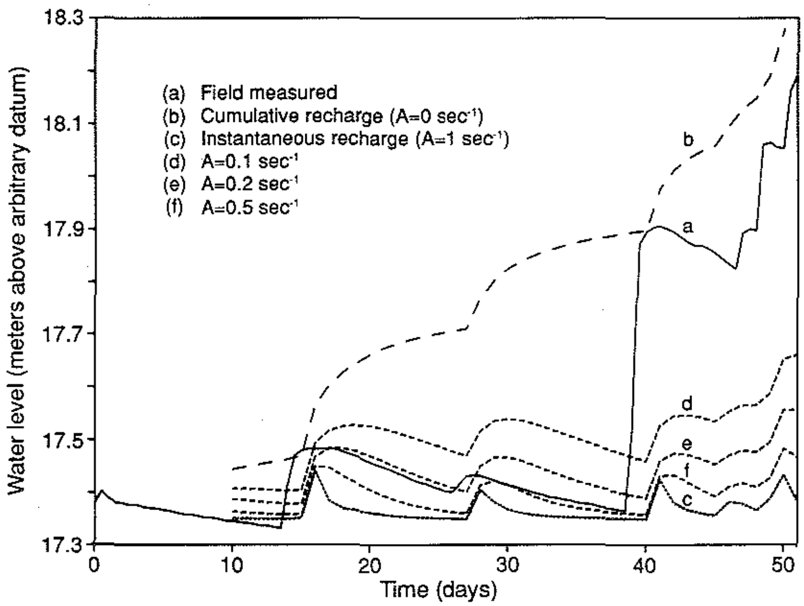

Figure 18. Water-table elevation versus time (measured and simulated). Curve a is the water-table elevation measured in the field at an observation well 20 km east of the study site (see Stoertz, 1985). Curve b is a simulated water level assuming no background water-table decline; recharge is cumulative (A = 0 sec^{-1} in equation 16). Curve c is instantaneous recharge (A = 1 sec^{-1} in equation 16). Note that figures 15 and 20-23 can be interpreted as plots of instantaneous recharge. Curves d, e, and f assume different degrees of background water-table decline: A = 0.1 sec^{-1}, 0.2 sec^{-1}, and 0.5 sec^{-1} in equation 16. All water levels are in meters above an arbitrary datum set 20 m below the land surface.

recharge; and (2) that the weighting factor for any given day of recharge declines exponentially with elapsed time. Combining these assumptions yields equation 16, which describes head as a function of time.

$$h_i = \sum_{n=0}^{i} Q_{i-n}\, e^{-nAt}, \qquad (16)$$

where h_i is head in cm on day i, Q is total recharge in cm during the elapsed time in seconds equal to it, and A is a parameter to be determined (sec^{-1}).

Figure 18, curve a, shows the measured water level at site 2 for the 51-day simulation period 8/29/84 to 10/16/84. Five simulated water levels also are shown in figure 18, curves b to f. In figure 18b, A = 0 sec^{-1}, so recharge is cumulative (all previous days of recharge are fully weighted). In figure 18c, A = 1 sec^{-1}. In this case, only the current day of recharge is weighted, and the resulting water level is the same as a drainage curve, such as those shown in figures 15 and 20 to 23 (with corrections for units). More realistic cases are figure 18d, e, and f, in which different degrees of decay are assumed: A = 0.1 sec^{-1}, 0.2 sec^{-1}, and 0.5 sec^{-1}, respectively. The simulated water levels of figure 18e (A = 0.2 sec^{-1}) fit the measured water levels reasonably well, up to about day 38. The rapid rise in measured water levels at day 38 indicates an external source of water,

Figure 19. Illustration of four soil tension versus depth profiles discussed in the text as possible steady-state initial conditions for simulations. Curve a (solid) is a hypothetical hydrostatic profile in which the tension balances the elevation head, assuming no infiltration. Curves b, c, and d are steady-state tension profiles with constant infiltration. Infiltration rates *R* are shown on the graph. Corresponding tensions and moisture contents are (b) $\psi = -100.4$ cm, $\theta = 0.073$; (c) $\psi = -110.0$ cm, $\theta = 0.062$; and (d) $\psi = -120.4$ cm, $\theta = 0.053$.

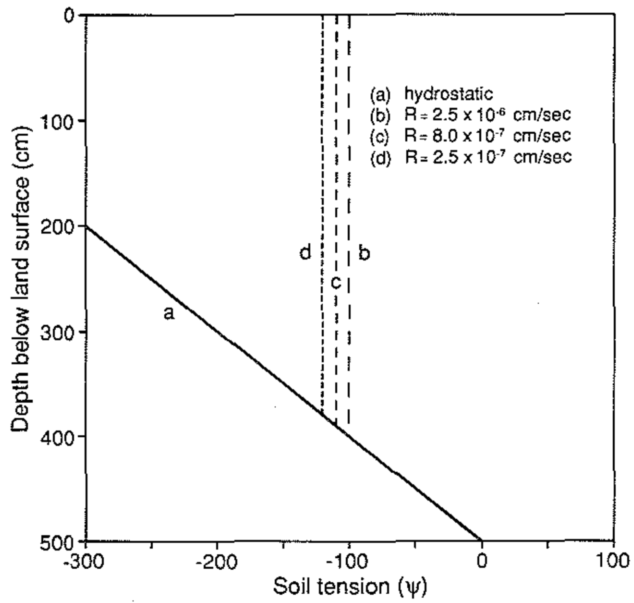

which we suggest comes from upgradient in the regional flow system. The simplified model presented here assumes no lateral flow, except implicitly in the regional decay term.

The model is able to simulate water-table fluctuations within the discretization error. (Measured water levels are discretized into half-day intervals; recharge is discretized into one-day intervals.) The model may predict the magnitude of response to individual storms, provided regional sources of water do not overwhelm unsaturated-zone sources. This conclusion suggests that the model may successfully predict water-table rises in recharge areas, particularly those at the upper end of a flow system.

Influence of antecedent soil moisture on recharge

The initial conditions used in modeling a storm (or series of storms) are equivalent to the antecedent soil moisture. Therefore, antecedent soil moisture is discussed here in the context of choosing appropriate initial conditions in unsaturated flow modeling.

Ideally, initial conditions correspond to field-observed tension (or moisture content converted to tension with the characteristic curve). However, field-observed tension may not be available or may not be mathematically consistent with the flow model. For example, a model may exclude heterogeneities, and field tension arising from those heterogeneities will never be reproduced by the model. Field tension may be best used as a guide in choosing initial conditions mathematically consistent with the model.

Initial conditions can be chosen several different ways:

• Initial tension corresponding to a steady-state profile with no infiltration can be used (curve a in fig. 19). This hydrostatic condition will have extremely high tension in the upper nodes if the soil is thick because the tension must offset the elevation head. Such high tension may never be observed in the field except in the plant root zone where osmotic gradients exist. Therefore, it is

Figure 20. Simulated drainage over a 51-day period for the same infiltration applied to four 500 cm thick soil profiles with different antecedent soil moisture (different initial conditions). Curves b, c, and d correspond to the steady-state initial conditions shown in figure 19; that is, ψ = -100.4 cm, -110.0 cm, and -120.4 cm, respectively.

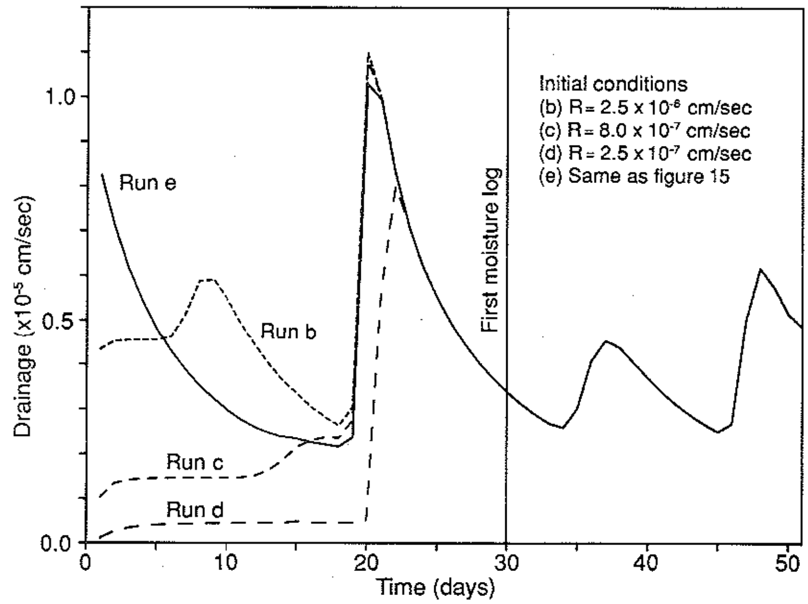

not recommended that this type of initial condition be used for applications in humid areas like Wisconsin.

- Initial tension corresponding to a steady-state profile with constant infiltration can be used (fig. 19b, c, d). The infiltration rate is converted to an initial tension by recognizing that the conductivity will just equal the infiltration rate [$K(\psi) = R$]. A tension corresponding to that conductivity is calculated from the $K(\psi)$ function (equation 10 or fig. C2). Three simulations with initial conditions corresponding to three steady infiltration rates are shown in figure 20b, c, and d. In the first simulation R is equal to 2.5×10^{-6} cm/sec, the average daily rain intensity based on an annual precipitation of 78 cm. Because $K(\psi) = 2.5 \times 10^{-6}$ cm/sec, $\psi = -100.4$ cm, using equation 10. In the second simulation, R is about one-third of the previous case, based on the assumption that only about one-third of annual precipitation becomes net infiltration. In the third simulation, R is arbitrarily made one-tenth of its value in the first simulation.

- Initial tension can be taken from a model-generated profile. For example, in the verification step of the previous section we used the 26-day profile as an initial condition (fig. 20e) because it followed a long period without rain.

Because the different ways of handling initial conditions give different recharge rates for early times in the simulation, these early rates must be interpreted cautiously (or ignored altogether). With time and in particular with intervening storms, the influence of the initial conditions becomes negligible.

Using steady-state initial conditions with constant infiltration produces a long-duration recharge event at early times in the simulation unless the steady-state infiltration used to establish the initial conditions is very small. A small infiltration rate, however, results in a dry soil column so that the lag time between the first rainfall event and its recharge pulse may be unrealistically long (several weeks or more) due to the low hydraulic conductivity under dry conditions. The lag time for later pulses decreases once the first major event has penetrated to the water table, wetting the soil column.

To avoid the problems discussed above, the start of the simulated period can be extended backward in time to incorporate an earlier major storm. The initial conditions for the extended period are then less critical provided initial conditions are not excessively dry. The time period of interest (excluding the early storm) will then have an initial condition generated by and therefore consistent with the model. We used this approach in the model verification because the first moisture profile is at 30 days, preceded by the storm at 15 days, which erased the effect of the initial conditions (fig. 15).

Influence of depth to water on recharge

The thickness of the unsaturated zone (the depth to the water table) profoundly influences the timing of recharge pulses and their amplitudes. To test this influence we changed the thickness of the soil column from 500 cm to 250 cm and then to 750 cm and calculated drainage (fig. 21). Initial conditions were chosen to represent steady infiltration at 8 x 10^{-7} cm/sec. Table 5 summarizes the results of the simulations. For the shallow 250 cm profile (curve a in fig. 21), the recharge pulse appears at the water table from 1 to 3 days after the storm, and the response (recharge pulse height divided by storm intensity) is 22 to 24 percent. For the 500 cm profile (curve b in fig. 21), the lag time between rainfall and recharge is 5 to 11 days, with a response between 8 and 12 percent. For the deep 750 cm profile (curve c in fig. 21) the lag time is 12 days or more, and the response is from 5 to 10 percent. If the very dry initial conditions of figure 19d are used, the lag between rainfall and recharge for storm 1 increases for the three profile depths. The lag times for the remaining storms are unchanged, which confirms that model results for the first storm should

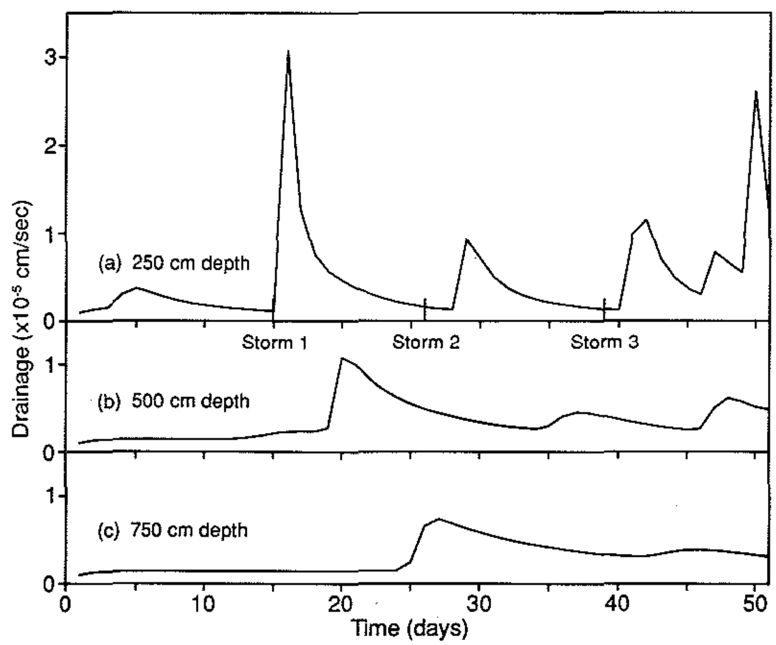

Figure 21. Simulated drainage over a 51-day period for the same infiltration applied to three soil thicknesses: 250 cm, 500 cm, and 750 cm. The time scale is the same for all three curves, and the times of the three major storms are shown on the upper time scale. A thicker soil delays and attenuates the recharge pulse relative to the rainfall event.

Table 5. Summary of simulations to test the influence of soil depth on the timing and the magnitude of the recharge pulse. The lag time is the number of days between a storm event and its associated recharge pulse; the response is the peak recharge rate divided by the storm intensity.

Depth of soil (cm)	Lag for storm 1 (days)	Lag for storm 2 (days)	Lag for storm 3 (days)	Response storm 1 (%)	Response storm 2 (%)	Response storm 3 (%)
250	1	3	3	0.22	0.24	0.22
500	5	11	9	0.08	0.12	0.12
750	12	19	-	0.05	0.10	-

be used cautiously. The long lag times observed for the 500 cm and 750 cm profiles suggest that even in permeable soils a substantial amount of water may be retained in the unsaturated zone for several weeks after a large storm, particularly if the soil was initially dry.

Influence of storm size on recharge

To demonstrate the influence of storm size on the recharge pulse, the model was run with the initial condition used in the model verification (fig. 20, curve e). The profile was allowed to drain for ten days before starting infiltration for a period up to 24 hours. Drainage rates were plotted starting at the initiation of infiltration and continuing for another 30 days. In figure 22 the storm intensity varies from 3×10^{-5} cm/sec to 9×10^{-5} cm/sec; the duration of the storm is held constant at 12 hours. In figure 23, storm duration varies from 7 to 22 hours; intensity is held constant at 9×10^{-5} cm/sec. These realistic intensities and durations are based on observations of storms in 1984.

Intensity affects the timing and magnitude of the drainage pulse. As expected, more intense storms cause the pulse to appear at the water table earlier, and the peak drainage rate is higher (fig. 22). A long-duration storm causes earlier drainage-pulse arrival relative to a shorter-duration storm of the same intensity (fig. 23). The longer duration allows fuller wetting of the profile, increasing the hydraulic conductivity and thereby moving the pulse through the column rapidly.

Because long-duration storms may be less intense than short cloudbursts, we

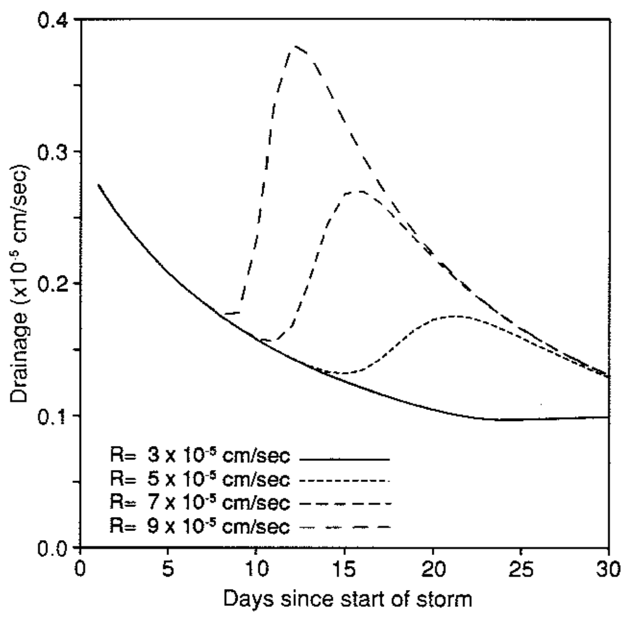

Figure 22. Drainage resulting from four simulations using infiltration rates (R) of 3×10^{-5} cm/sec, 5×10^{-5} cm/sec, 7×10^{-5} cm/sec, and 9×10^{-5} cm/sec, with a constant duration of 12 hours. The model is the calibrated 500 cm thick model used elsewhere in this paper.

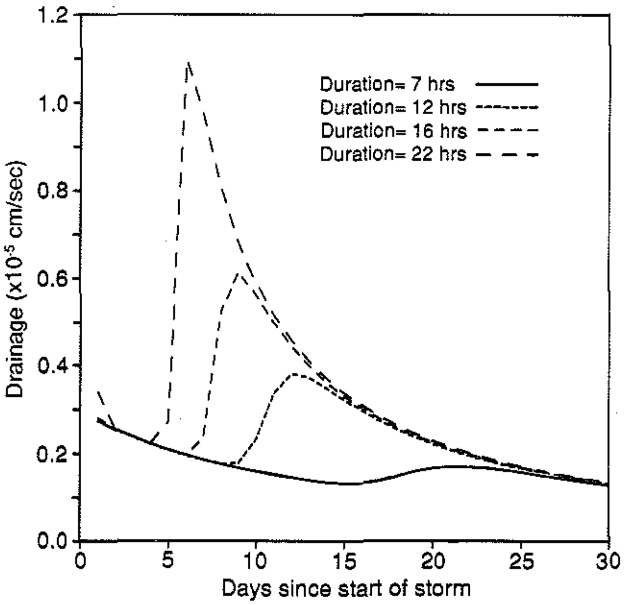

Figure 23. Drainage resulting from four simulations using storm durations of 7, 12, 16, and 22 hours, with a constant intensity of 9 x 10^{-5} cm/sec. The model is the calibrated 500 cm thick model used elsewhere in this paper.

compared the drainage in two simulations resulting from 6 cm of rain applied over a 24-hour period and a 1-hour period. The long-duration, low-intensity storm resulted in a drainage pulse arriving three days before the pulse from the short-duration, high-intensity storm. The long-duration storm results in more drainage for the first several weeks after the storm. Ultimately, both storms will generate 6 cm of drainage in the absence of evapotranspiration.

Watson (1986) modeled a 6 m column of medium to fine sand (K_{SAT} = 1.3 x 10^{-4} m/sec), applying 10 cm of water to the top of the column during a 50-minute period, and found that the recharge pulse arrived at the water table in 29 hours. Using a coarser sand and the same input of water, the wetting front reached a depth of 5 m after about 8 hours. Watson's (1986) input pulses (3 x 10^{-3} cm/sec for 0.8 hours; 10 cm total) are much larger than the rain pulse shown in figures 22 and 23 (maximum 9 x 10^{-5} cm/sec for 12 hours; 4 cm total), so recharge pulses occur after a much shorter lag time. The instantaneous profile test represents an input pulse of 3.5 x 10^{-3} cm/sec for 6 hours (75 cm total), and the wetting front reached a depth of 5 m after 6 hours. The short lag times reported by Watson (1986) and reported here for the instantaneous profile test are not representative of real rain storms, so the lag times shown in figures 22 and 23 are thought to be more realistic.

DISCUSSION

According to Freeze (1969), natural recharge and discharge can be viewed from the perspective of the regional flow system in which the water table is a manifestation of the various inputs and withdrawals, or from the perspective of the unsaturated zone, which provides the driving sources and sinks of water. We have used both approaches in our recharge study. This paper is a summary of methods and conclusions from the unsaturated zone perspective. Bradbury and others (in press) and Stoertz and Bradbury (1989) discussed results from the regional flow system perspective.

Considering the expense and complexity of studying the unsaturated zone relative to the regional saturated flow system, we found our regional saturated flow studies (Bradbury and others, in press; Stoertz and Bradbury, 1989) to be more fruitful and less subject to errors. In particular, the uncertainties in evaporation rates needed for an unsaturated flow model and the problems in spatial extrapolation make precise estimates of recharge difficult. Nevertheless, as mentioned in the introduction to this paper, there are cases in which monitoring the unsaturated zone is necessary. The most justifiable cases are those for which leachate tracking or recharge estimates at a site are needed.

Assumptions and their implications

Users of this model or similar models should be wary of the numerous assumptions required to make the problem manageable.

- The methodology that we developed is designed mainly to estimate the total groundwater recharge volume and timing after heavy precipitation. Whether the majority of the contaminants leached into the groundwater are carried by such heavy precipitation events is unknown.
- The water-table boundary at the bottom of the modeled soil column is stationary. If one is interested in calculating recharge rates as influenced by water-table fluctuations, the model must be modified (for example, see Freeze, 1969).
- The model treats only the homogeneous case. If the profile to be modeled is layered, the model must be modified. The effects of the assumption of homogeneity can be seen in comparing the modeled moisture profiles (fig. 12) with the measured profiles (fig. 6). The actual soil profile has low-conductivity layers at the surface and at a depth of about 175 cm. The high moisture content that results from the conductivity contrasts is not reproduced by the model.
- The model is designed for a constant-flow upper boundary. If a ponded condition is to be simulated, the model must be modified. Although we observed ponding at the surface during the instantaneous profile test, it was due to the low-conductivity surface layer, and we believe that a constant-flux condition existed just below the surface layer.
- The model does not simulate evapotranspiration, which reduces recharge significantly. We justify neglecting evapotranspiration by simulating a series of rainstorms that occurred during the fall. Moreover, the site used for verification is bare of vegetation, and no roots were encountered during drilling. If evapotranspiration cannot be ignored, the data needs are increased substantially and the model must be modified.
- The model neglects hysteresis in the water retention curves and uses only a draining curve. Errors in moisture content and gradient values can be large for early times in redistribution of water in sand if draining curves are used where hysteresis is important. However, at later times, on the order of several hours, the error is small. The qualitative effect of using a draining curve instead of a hysteretic curve is that recharge will arrive several hours sooner if the draining curve is used. Stephens and Knowlton (1986) commented that neglecting hysteresis (using a draining curve during a wetting cycle) in their study of recharge through sand in New Mexico resulted in overestimating recharge. Pickens and Gillham (1980) modeled post-infiltration moisture redistribution in a fine sand with and without hysteresis, and their results show that the maximum error in moisture content using a draining curve rather than allowing for hysteresis was about 3 percent and the maximum error in tension was about 20 cm.

• We accounted for lateral flow only by reducing the infiltration rate in the model calibration but did not model it explicitly during the instantaneous profile test. This does not affect the curves derived from the test, but measurements of water applied during the test (if used as infiltration rates in the unsaturated model) seem to be too high: the resulting measurements of steady-state moisture are much higher than those observed during the test. Rough calculations suggest that as much as 60 percent of the added water did not remain directly below the plot, but flowed laterally. Lateral flow is expected in fine soils, but well sorted medium sands are often assumed to transmit water only vertically. This may not be a good assumption, especially in cases where layering occurs, even though the conductivity contrasts are subtle (S. Kung, University of Wisconsin-Madison, Department of Soil Science, written communication, 1988).

• The air phase is assumed to have no effect on infiltration. This assumption is probably justified because soil permeability is so large that ponding almost never occurs; the soil is rarely saturated. During the instantaneous profile test, water was applied at more than 10 cm/hr for 6 hours, so ponding occurred. However, because the ponded area was limited, air could flow freely laterally and was probably not entrapped.

• We assumed that the soil reached equilibrium with the tensiometer cups at all times. This assumption is necessary because better ways of measuring soil tension are not available. The delay in response of the commercial tensiometers suggests that the soil does not always reach equilibrium with tensiometers rapidly. However, the transducer tensiometers responded rapidly and stabilized (fig. 8), so we feel the assumption is valid in this case. For natural rainstorms, moisture changes are generally not as rapid as they were during the test, and the commercial tensiometers should have time to equilibrate.

• Temperature effects are assumed to be negligible, which is probably valid for coarse-grained materials. Temperature effects may be significant in fine-textured soils (Nielsen and others, 1986).

• The model assumes an incompressible soil matrix and a fluid consisting of pure water. The model ignores the effects of fluid density. These assumptions are reasonable because sand is relatively incompressible and the ionic strength of the water is very low.

CONCLUSIONS

This study yields the following conclusions:

• The instantaneous profile method is an effective technique for developing soil characteristic curves in the sand plain of central Wisconsin and similar areas.

• Obtaining accurate hydraulic head data in the unsaturated zone in the sand plain requires specially designed, quickly responding tensiometers linked to a datalogger.

• A calibrated numerical unsaturated flow model can be used to calculate deep drainage from the unsaturated zone.

• The unsaturated model is somewhat successful in reproducing water-table responses to recharge. In predicting the water-table hydrograph, regional influences on the water table must be taken into consideration. Assuming an exponential decline of the water level with time to account for regional flow is a promising approach.

• Groundwater recharge in the sand plain appears to be controlled by major storms. Recharge is greatest following high-intensity, long-duration storms. However, a short-duration, high-intensity storm can produce the same recharge as a long-duration, low-intensity storm.

• For a 5 m thick unsaturated zone in the sand plain, recharge pulses are unlikely to occur sooner than one week after a storm, and in many cases the lag time before the recharge peaks may exceed one month.

Recommendations

Specific suggestions for equipment design are included in the section on methodology.

The computer code used here (appendix A) is intended primarily for demonstrating the principles of unsaturated flow modeling, or for carrying out simple modeling for cases in which the assumptions inherent in the code (for example, homogeneity, negligible hysteresis, fixed water table, constant-flux upper boundary condition) are warranted. This model could be modified to allow for more complex one-dimensional simulations. However, we caution the user that the model has not been validated against an analytical solution or other numerical models to check for inconsistencies or numerical problems. We recommend that a documented public-domain model be used rather than the simple and relatively inflexible model included here. Many unsaturated flow codes are quite sophisticated, allowing for solute or heat transport and aquifer compressibility as well as flow. A summary of variably saturated flow models is given by Lappala (1981). Available models include SUTRA (Voss, 1984), VS2D (Lappala and others, 1987), UNSAT2 (Davis and Neuman, 1983), 3DFEMWATER (Yeh, 1987), and SWATRE (Belmons and others, 1983).

REFERENCES

Ahuja, L.R. and S.A. El-Swaify, 1979, Determining soil hydrologic characteristics on a remote forest watershed by continuous monitoring of soil-water pressures, rainfall and runoff: *Journal of Hydrology,* vol. 44, p. 135-147.

Ahuja, L.R., R.E. Green, and S.K. Chong, 1980, A simplified functions approach for determining soil hydraulic conductivities and water characteristics in situ: *Water Resources Research,* vol. 16, no. 5, p. 947-953.

Baker, F.G., 1978, Variability of hydraulic conductivity within and between nine Wisconsin soil series: *Water Resources Research,* vol. 14, no.1, p. 103-108.

Bartelme, R.J., 1977, Soil Survey of Wood County, Wisconsin: U.S. Department of Agriculture, Soil Conservation Service, in cooperation with Wisconsin Research Division, College of Agricultural and Life Sciences, University of Wisconsin, 106 p. plus plates.

Belmans, C., J.G. Wesseling, and R.A. Feddes, 1983, Simulation model of the water balance of a cropland soil: SWATRE: *Journal of Hydrology,* vol. 63, p. 271-286.

Bouma, J., F.G. Baker, and P.L.M. Veneman, 1974, Measurement of water movement in soil pedons above the water table: Wisconsin Geological and Natural History Survey Information Circular 27, 113 p.

Bouma, J. and J.L. Denning, 1974, A comparison of hydraulic conductivities calculated with morphometric and physical methods: *Soil Science Society of America Proceedings,* vol. 38, p. 124-127.

Bradbury, K.R., and M.A. Muldoon, 1990, Hydraulic conductivity determinations in unlithified glacial and fluvial materials, in Nielsen, D.M., and Johnson, A.I., eds., *Groundwater and Vadose Zone Monitoring, ASTM STP 1053*: American Society for Testing and Materials, Philadelphia, PA, p. 138-151.

Bradbury, K.R., M.W. Stoertz, and J.M. Faustini, in press, Groundwater recharge and groundwater flow systems in the Buena Vista Groundwater Basin, Portage and Wood Counties, Wisconsin: Wisconsin Geological and Natural History Survey Information Circular 72.

Brooks, R.H., and A.T. Corey, 1964, Hydraulic properties of porous media: Hydrology Papers 3, Colorado State University, Fort Collins, Colorado, 27 p.

Brownell, J.R., 1986, Stratigraphy of unlithified deposits in the Central Sand Plain of Wisconsin: M.S. thesis, University of Wisconsin, Madison, 172 p.

Brutsaert, W., 1966, Probability laws for pore size distribution: *Soil Science,* vol. 101, p. 85-92.

Cichowicz, N.L. 1979, Development and application of a linked unsaturated-saturated flow model: M.S. thesis, University of Wisconsin, Madison, 98 p.

Clayton, L., 1986, Pleistocene geology of Portage County, Wisconsin: Wisconsin Geological and Natural History Survey Information Circular 56, 19 p.

Darcy, H., 1856, *Les fontaines publiques de la ville de Dijon:* Victor Dalmont, Paris.

Davis, S.N., and R.J.M. DeWiest, 1966, *Hydrogeology:* John Wiley and Sons, 463 p.

Davis, L.A., and S.P. Neuman, 1983, Documentation and user's guide: UNSAT2 variably saturated flow model (including four example problems): NUREG/CR-3390 WWL/TM1791-1, U.S. Nuclear Regulatory Commission, 200 p.

Denning, J.L., J. Bouma, O. Falayi, and D.J. Van Rooyen, 1974, Calculation of hydraulic conductivities of horizons in some major soils in Wisconsin: *Geoderma,* vol. 11, p. 1-16.

Douglas, J., and B.F. Jones, 1963, On predictor-corrector methods for nonlinear parabolic differential equations: *Journal of the Statistics Institute of America,* vol. 11, p. 195-204.

Dreiss, S.D., and L.D. Anderson, 1985, Estimating vertical soil moisture flux at a land treatment site. *Ground Water,* vol. 23, no. 4, p. 503-511.

Dutton, C.E., and R.E. Bradley, 1970, Lithologic, geophysical and mineral commodity maps of Precambrian rocks in Wisconsin: U.S. Geological Survey Miscellaneous Geological Investigations Map I-631, 6 sheets, scales 1:500,000 and 1:1,000,000.

Enfield, C.G., J.J.C. Hsieh, and A.W. Warrick, 1973, Evaluation of water flux above a deep water table using thermocouple psychrometers: *Soil Science Society of America Proceedings,* vol. 37, p. 968-970.

Fayer, M.J., and D. Hillel, 1982, Field testing of a two-dimensional soil moisture model simulating water table fluctuations: *Soil Science Society of America Journal,* vol. 46, p. 396-404.

Freeze, R.A., 1969, The mechanism of natural ground-water recharge and discharge - 1. One-dimensional, vertical, unsteady, unsaturated flow above a recharging or discharging ground-water flow system: *Water Resources Research,* vol. 5, no. 1, p. 153-171.

Freeze, R.A., 1971, Three-dimensional, transient, saturated-unsaturated flow in a groundwater basin: *Water Resources Research,* vol. 7, no. 2, p. 347-366.

Freeze, R.A., and J. Banner, 1970, The mechanism of natural ground-water recharge and discharge - 2. Laboratory column experiments and field measurements: *Water Resources Research,* vol. 6, no. 1, p. 138-155.

Freyberg, D.L., J.W. Reeder, J.B. Franzini, and I. Remson, 1980, Application of the Green-Ampt model to infiltration under time-dependent surface water depths: *Water Resources Research,* vol. 16, no. 3, p. 517-528.

Frind, E.O., and M.J. Verge, 1978, Three-dimensional modeling of groundwater flow systems: *Water Resources Research,* vol. 14, no. 5, p. 844-856.

Gee, G.W., and R.R. Kirkham, 1984, Arid site water balance: Evapotranspiration modeling and measurements, Report PNL - 5177: Pacific Northwest Laboratories, Richland, Washington, 38 p.

Hillel, D., V.D. Krentos, and Y. Stylianou, 1972, Procedure and test of an internal drainage method for measuring soil hydraulic characteristics in situ: *Soil Science,* vol. 114, no. 5, p. 395-400.

Hole, F.D., 1976, *Soils of Wisconsin:* University of Wisconsin Press, 223 p.

Holt, C.L.R., Jr., 1965, Geology and water resources of Portage County, Wisconsin: U.S. Geological Survey Water-Supply Paper 1796, 77 p.

Jones, A.J. and R.J. Wagenet, 1984, In situ estimation of hydraulic conductivity using simplified methods: *Water Resources Research,* vol. 20, no. 11, p. 1620-1626.

King, L.G., 1965, Description of soil characteristics for partially saturated flow: *Soil Science Society of America Proceedings,* vol. 29, no. 4, p. 359-362.

Kovacs, G., 1986, Methods to characterize groundwater-atmosphere interactions: Conjunctive Water Use: Proceedings of the Budapest Symposium, July 1986, IAHS Publication 156, p. 259-276.

Krishnamurthi, N., D.K. Sunada, and R.A. Longenbaugh, 1977, Mathematical modeling of natural groundwater recharge: *Water Resources Research,* vol. 13, no. 4, p. 720-724.

Lappala, E.G., 1981, Modeling water and solute transport under variably saturated conditions: State of the art: Proceedings of the Interagency Workshop on Modeling and Low Level Waste management: An Interagency Workshop, Denver, Colorado, Dec. 1980, p. 81-137.

Lappala, E.G., R.W. Healy, and E.P. Weeks, 1987, Documentation of computer program VS2D to solve the equations of fluid flow in variably saturated porous media: U.S. Geological Survey Water-Resources Investigations Report 83-4099, 184 p.

Lawrence, A.R., and H.A. Dharmagunawardena, 1983, Vertical recharge to a confined limestone in northwest Sri Lanka: *Journal of Hydrology,* vol. 63, p. 287-297.

Masch, F.D., and K.J. Denny, 1966, Grain size distribution and its effect on the permeability of unconsolidated sands: *Water Resources Research,* vol. 2, no. 4, p. 665-677.

Nielsen, D.R., M. Th. Van Genuchten, and J.W. Biggar, 1986, Water flow and solute transport processes in the unsaturated zone: *Water Resources Research,* vol. 22, no. 9, p. 805-1085.

Nixon, P.R., and G.P. Lawless, 1960, Detection of deeply penetrating rain water with neutron-scattering moisture meter: *Transactions of the American Society of Agricultural Engineers,* vol. 3, no. 1, p. 5-8.

Nnyamah, J.V., and T.A. Black, 1977, Rates and patterns of water uptake in a Douglas fir forest: *Soil Science Society of America Journal,* vol. 41, p. 972-979.

Pickens, J.F., and R.W. Gillham, 1980, Finite element analysis of solute transport under hysteretic unsaturated flow conditions: *Water Resources Research,* vol. 16, no. 6, p. 1071-1078.

Pikul, M.F., 1973, Numerical studies of linked soil-moisture and groundwater systems: Ph.D. thesis, Stanford University, 92 p.

Pikul, M.F., R.L. Street, and I. Remson, 1974, A numerical model based on coupled one-dimensional Richards and Boussinesq equations: *Water Resources Research,* vol. 10, no. 2, p. 295-302.

Reeder, J.W., D.L. Freyberg, J.B. Franzini, and I. Remson, 1980, Infiltration under rapidly varying surface water depths: *Water Resources Research,* vol. 16, no. 1, p. 97-104.

Richards, L.A., 1931, Capillary conduction of liquids through porous mediums: *Physics,* vol. 1, p. 318-333.

Richards, L.A., 1965, Physical condition of water in soil, *in* C.A. Black, ed., *Methods of Soil Analysis,* Part 1, Agronomy 9, 128-152: American Society of Agronomists, Madison, Wisconsin.

Rubin, J., 1966, Theory of rainfall uptake by soils initially drier than their field capacity and its applications: *Water Resources Research,* vol. 2, no. 4, p. 739-749.

Rubin, J., 1967, Numerical method for analyzing hysteresis-affected, post-infiltration redistribution of soil moisture: *Soil Science Society of America Proceedings,* vol. 31, p. 13-20.

Schmugge, T.J., T.J. Jackson, and H.L. McKim, 1980, Survey of methods for soil moisture determination: *Water Resources Research,* vol. 16, no. 6, p. 961-979.

Soilmoisture Equipment Corporation, Santa Barbara, California, no date, Principles involved in the operation of a tensiometer type measuring instrument: Article 6.

Sophocleus, M., and C.A. Perry, 1984, Experimental studies of natural groundwater recharge dynamics: Assessment of recent advances in instrumentation: *Journal of Hydrology,* vol. 70, p. 369-382.

Sophocleus, M. and C.A. Perry, 1985, Experimental studies in natural groundwater recharge dynamics: The analysis of observed recharge events: *Journal of Hydrology,* vol. 81, p. 297-332.

Steenhuis, T.S., C.D. Jackson, S.K.J. Kung, and W. Brutsaert, 1985, Measurement of groundwater recharge on eastern Long Island, New York, U.S.A.: *Journal of Hydrology,* vol. 79, p. 145-169.

Stephens, D.B. and R. Knowlton, Jr., 1986, Soil water movement and recharge through sand at a semiarid site in New Mexico: *Water Resources Research,* vol. 22, no. 6., p. 881-889.

Stoertz, M.W., 1985, Evaluation of groundwater recharge in the Central Sand Plain of Wisconsin: M.S. thesis, University of Wisconsin, Madison, 159 p.

Stoertz, M.W., and K.R. Bradbury, 1989, Mapping recharge areas using a groundwater flow model – a case study: *Ground Water,* vol. 27, no. 2, p. 220-228.

Topp, G.C., 1969, Soil-water hysteresis measured in a sandy loam and compared with the hysteretic domain model: *Soil Science Society of America Proceedings,* vol. 33, p. 645-651.

Vauclin, M., D. Khanji, and G. Vachaud, 1979, Experimental and numerical study of transient two-dimensional unsaturated-saturated water table recharge pattern: *Water Resources Research,* vol. 15, no. 5, p. 1089-1101.

Voss, C.I., 1984, A finite-element simulation model for saturated-unsaturated, fluid-density-dependent groundwater flow with energy transport or chemically-reactive single-species solute transport: U.S. Geological Survey Water-Resources Investigations Report 84-4369, 409 p.

Watson, K.K., 1966, An instantaneous profile method for determining the hydraulic conductivity of unsaturated porous materials: *Water Resources Research,* vol. 2, no. 4, p. 709-715.

Watson, K.K., 1986, Numerical analysis of natural recharge to an unconfined aquifer: Conjunctive water use: Proceedings of the Budapest Symposium, July 1986, IAHS Publication 156, p. 323-333.

Wellings, S.R., 1984, Recharge in the Upper Chalk Aquifer at a site in Hampshire, England: *Journal of Hydrology,* vol. 69, p. 259-273.

Wilson, L.G., 1981, Monitoring in the vadose zone Part I: Storage changes: *Ground Water Monitoring Review,* Fall 1981, p. 32-41.

Winter, T.C., 1983, The interaction of lakes with variably saturated porous media: *Water Resources Research,* vol. 19, no. 5, p. 1203-1218.

Yeh, G.T., 1987, 3DFEMWATER: A three-dimensional finite-element model of water flow through saturated-unsaturated media: Oak Ridge National Laboratories, Environmental Sciences Division, Publication 2904, 314 p.

APPENDIX A. Code listing

```
C**********************************************************************
C  UU          UU   NNN       NN     SSSSS       AAAAAA   TTTTTTTTTT    C
C  UU          UU   NNNN      NN   SS      SS   AA       AA      TT     C
C  UU          UU   NN NN     NN   SS      SS  AA        AA      TT     C
C  UU          UU   NN NN     NN     SS        AA        AA      TT     C
C  UU          UU   NN  NN    NN      SSSSS    AAAAAAAAA         TT     C
C  UU          UU   NN  NN    NN           SS  AA        AA      TT     C
C  UU          UU   NN    NN  NN   SS        SS AA       AA      TT     C
C    UU      UU     NN     NNNN     SS     SS  AA        AA      TT     C
C     UUUUUU        NN      NNN      SSSSS     AA        AA      TT     C
C**********************************************************************
C                                                                       C
C   ONE-DIMENSIONAL, HOMOGENEOUS, UNSATURATED GROUNDWATER               C
C   FLOW MODEL MODIFIED FROM CICHOWICZ (1979) AND PIKUL (1973).         C
C                                                                       C
C**********************************************************************
C
C                     Units are cm and sec throughout.
C
C                          LIST OF VARIABLES
C
C    A        Matrix array.
C    ACAP     Vector containing values of specific moisture capacity;
C                see Freeze and Cherry (1979, p. 62).
C    ACON     Vector containing values of unsaturated hydraulic conductivity.
C    ASMQ     Average rate of drainage from a soil column for a simulation period
C    B        Matrix array.
C    C        "
C    CONL1, CONL2, CONU1, CONU2       Vectors containing nodal averages of
C                unsaturated hydraulic conductivity. "L" means lower, "U" means
C                upper, "1" means N+1/2 time step, "2" means N time step.
C    DELT     Time increment.
C    DELZ     Nodal spacing in the z direction.
C    DIFF     Difference in moisture contents between the beginning and end of
C                a time step.
C    F        Matrix array used in subroutine TRIDIA.
C    IEND     Total number of time steps to be simulated.
C    ITER     Iteration counter.
C    KOUNT    Printing counter, reset after each printout.
C    KPNT     Number of time steps between printouts.
C    L        Counter for infiltration period.
C    M1       Number of the first node above the water table.
C    MM       Number of the node at the top of the soil column.
C    NPER     Number of periods with different infiltration rates.
C    PARA1, PARB1, PARN  Parameters A, B, and N in Brutsaert's empirical
C                equations; Wet part of spliced curve.
C     PARA2, PARB2  Parameteers A, B in Brutsaert's empirical equations;
C                Dry part of spliced curve.
C    PER(L)   Lth infiltration period.
C    PSI1, PSI2   Vectors containing values of pressure head
C                in the main program.
C    PSTOR    Amount of water stored in a segment (DELZ) of soil column.
C    R        Infiltration rate.
C    RR(L)    Rate (cm/sec) for Lth infiltration period.
C    RHS      Right-hand side of equation.
C    SATK     Hydraulic conductivity at saturation.
C    SATTH    Moisture content at saturation.
C    SMQ      Rate of drainage out of a column during a time step.
C    SPYD     Specific yield.
C    STOR     Rate of change in storage for a column during a time step.
C    TDAYS    Time converted to days.
C    TPSI1    Temporary holding vector for the PSI1( ) vectors.
C    THETAI   Vector containing values of initial moisture contents.
C    THETAR   Retention moisture content at very high tensions.
C    THETA1   Vector containing moisture content values at the beginning
C                of a time step.
C    THETA2   Vector containing moisture content values at the end of a
C                time step.
C    TIME     Cumulative length of time.
```

```
C     TLEAST  Minimum value of moisture content in a soil column.
C     TR      Total infiltration (part of mass balance check).
C     TSTOR   Total storage change (part of mass balance check).
C     TSMQ    Total rate of drainage from a column for a simulation period.
C     X       Matrix array used in TRIDIA.
C     XPT     Cross-point tension where characteristic curve is spliced.
C     Z, ALPHA, BETA    Matrix arrays used in TRIDIA.
C
C      Subroutine TRIDIA — solves the Thomas Algorithm for the tridiagonal
C                   matrices.
C
C*******************************************************************
C
C     Allocate space and indicate variables common to main
C     code and subroutine.
C
      INTEGER PER(100)
      COMMON A,B,C,RHS,PSI2,Z,ALPHA,BETA,DELZ,THETAI,
     1 SATK,SATTH,M1,MM,KPNT,DELT,R,RR,TSTOR,
     2 STOR,SMQ,PSI1,TPSI1,TIME,SPYD,TLEAST
      DIMENSION A(100),B(100),C(100),RHS(100),PSI2(100)
      DIMENSION Z(100),ALPHA(100),BETA(100),RR(100)
      DIMENSION PSI1(100),TPSI1(100)
      DIMENSION ACON(100),ACAP(100),CONU1(100),CONL1(100)
      DIMENSION THETAI (100),CONU2(100),CONL2(100)
      DIMENSION THETA1(100),THETA2(100)
C
C     Format statements for printing.
C
 601  FORMAT  (8F10.6)
 602  FORMAT  (8I10)
 603  FORMAT  (F20.10)
 604  FORMAT  (E20.10)
 605  FORMAT  (6F20.5)
 606  FORMAT  (' ')
 608  FORMAT  (' ', '                 The time step is (sec)')
 609  FORMAT  (' ', '               Pressure heads (cm)')
 610  FORMAT  (' ', 'The infiltr. rates and corresponding iters. are')
 611  FORMAT  (' ', '         The rate of change of storage is')
 612  FORMAT  (' ', 'Rate of drainage out of the column (cm/sec)')
 613  FORMAT  (' ', '                 Moisture contents')
 614  FORMAT  (' ', '      Initial pressure heads (cm)')
 615  FORMAT  (8F10.2)
 616  FORMAT  (' ', '            Specific yield')
 617  FORMAT  (' ', '           Cumulative rate of drainage (cm/sec)')
 618  FORMAT  (8F10.4)
 619  FORMAT  (' ','           Average rate of drainage (cm/sec)')
 620  FORMAT  (' ','         Brutsaert parameters A1, B1, A2, B2, N')
 621  FORMAT  (I10,2F10.4)
 622  FORMAT  (' ', '                 Nodal spacing is (cm)')
 623  FORMAT  (' ', '           SATK (cm/sec), SATTH, THETAR  are')
 624  FORMAT  (' ', '    NODE  TIME(days)  THETA')
 625  FORMAT  (' ', 'TR (Total infiltration)')
 626  FORMAT  (' ', 'TSTOR (Total storage change)')
C
C     Read data from input file.
C
      READ  (5,602)  MM
      READ  (5,602)  M1
      READ  (5,602)  NPER
      READ  (5,601)  (RR(L),L=1,NPER)
      READ  (5,602)  (PER(L),L=1,NPER)
      READ  (5,603)  DELT
      READ  (5,603)  DELZ
      READ  (5,602)  IEND
      READ  (5,602)  KPNT
      READ  (5,603)  SATK
      READ  (5,603)  SATTH
      READ  (5,603)  THETAR
      READ  (5,615)  PARA1,PARB1,PARA2,PARB2,PARN
      READ  (5,603)  XPT
C
```

```
C     Echo input.
C
        WRITE  (6,608)
        WRITE  (6,603) DELT
        WRITE  (6,610)
        WRITE  (6,601) (RR(L),L=1,NPER)
        WRITE  (6,602) (PER(L),L=1,NPER)
        WRITE  (6,606)
        WRITE  (6,622)
        WRITE  (6,603) DELZ
        WRITE  (6,606)
        WRITE  (6,623)
        WRITE  (6,601) SATK, SATTH, THETAR
        WRITE  (6,620)
        WRITE  (6,605) PARA1,PARB1,PARA2,PARB2,PARN
C
        M=MM-1
        M2=M1+1
C
C     Read initial pressure heads.
C
        READ    (5,615) (PSI1(J),  J=M1,MM)
C
C     Calculate initial moisture contents from initial pressure
C     heads using moisture-tension characteristic curve. The curve
C     in the DO 10 loop is of the empirical form proposed by
C     Brutsaert. In this case, the curve is spliced from two curves
C     with different fitting parameters A and B.
C
        WRITE  (6,624)
        WRITE  (6,613)
        ZERO=0.0
        DO 10 J=M1,MM
          IF(PSI1(J).GE.XPT) THEN
            THETAI(J)=(SATTH-THETAR)*PARA1/(PARA1+((-PSI1(J))**PARB1))
     1      +THETAR
          ELSE
            THETAI(J)=(SATTH-THETAR)*PARA2/(PARA2+((-PSI1(J))**PARB2))
     1      +THETAR
          ENDIF
        WRITE(6,621) J,ZERO,THETAI(J)
 10     CONTINUE
C
        KOUNT=1
        TSMQ=0.0
        ASMQ=0.0
        TIME=0.0
C
C     Start iterating through time steps.  At appropriate times, change
C     the infiltration rates.
C
        L=1
        DO 20 ITER=1,IEND
          IF(ITER.GT.PER(L)) THEN
            R=RR(L)
            L=L+1
          END IF
          TIME=TIME+DELT
C
C     Set the pressure head at the water table equal to zero,
C     and set the hydraulic conductivity at the water table equal
C     to its value at saturation.
C
        PSI1(M1-1)=0.0
        PSI2(M1-1)=0.0
        ACON(M1-1)=SATK
C
C     For nodes above the water table, calculate the hydraulic
C     conductivity from the pressure head, using the K-psi curve.
C     Calculate the moisture content at start of time step, using the
C     moisture-tension characteristic curve.  The initial moisture
```

```
C     content will be used later to get the change in moisture content
C     during the time step.  Determine the specific moisture capacity.
C
        DO 30 J=M1,MM
          IF (PSI1(J).GE.0.0) THEN
            ACON(J)=SATK
            ACAP(J)=0.0
            THETA1(J)=SATTH
          ELSE IF (PSI1(J).GE.XPT) THEN
            ACON(J)=SATK*(PARA1/(PARA1+((-PSI1(J))**PARB1)))**PARN
            ACAP(J)=PARB1*(SATTH-THETAR)*PARA1+(-PSI1(J))**(PARB1-1.0)
            ACAP(J)=ACAP(J)/(PARA1+(-PSI1(J))**PARB1)**2.0
            THETA1(J)=(SATTH-THETAR)*PARA1/(PARA1+((-PSI1(J))**PARB1))
     1      +THETAR
          ELSE
            ACON(J)=SATK*(PARA2/(PARA2+((-PSI1(J))**PARB2)))**PARN
            ACAP(J)=PARB2*(SATTH-THETAR)*PARA2*(-PSI1(J))**(PARB2-1.0)
            ACAP(J)=ACAP(J)/(PARA2+(-PSI1(J))**PARB2)**2.0
            THETA1(J)=(SATTH-THETAR)*PARA2/(PARA2+((-PSI1(J))**PARB2))
     1      +THETAR
          ENDIF
 30   CONTINUE
C
C     Set up the unsaturated flow equations (see Pikul, 1973, p. 13).
C     The first part sets up the predictor.  A, B, and C are passed
C     to subroutine TRIDIA.
C
        DO 40 J=M1,M
          CONU1(J)=(ACON(J+1)+ACON(J))/2.0
          CONL1(J)=(ACON(J-1)+ACON(J))/2.0
          A(J)=CONL1(J)
          B(J)=-CONU1(J)-CONL1(J)-(ACAP(J)*2.0*DELZ**2/DELT)
          C(J)=CONU1(J)
          D1=2.0*ACAP(J)*PSI1(J)*DELZ**2/DELT
          RHS(J)=-D1-DELZ*(CONU1(J)-CONL1(J))
  40    CONTINUE
C
C     The top (MM) and bottom (M1) nodes of the column require special
C     treatment.
C
        RHS(M1)=RHS(M1)-PSI1(M1-1)*CONL1(M1)
        CONL1(MM)=(ACON(MM)+ACON(M))/2.0
        A(MM)=CONL1(MM)
        B(MM)=-CONL1(MM)-(2.0*ACAP(MM)*DELZ**2/DELT)
        D1=-2.0*ACAP(MM)*PSI1(MM)*DELZ**2/DELT
        D2=DELZ*(-R+CONL1(MM))
        RHS(MM)=D1+D2
C
        CALL TRIDIA (M1,M2,M,MM)
C
C     Set up the matrix of coefficients for the corrector.
C
        DO 50 J=M1,MM
          IF (PSI2(J).GE.0.0) THEN
            ACON(J)=SATK
            ACAP(J)=0.0
          ELSE IF (PSI2(J).GE.XPT) THEN
            ACON(J)=SATK*(PARA1/(PARA1+((-PSI2(J))**PARB1)))**PARN
            ACAP(J)=PARB1*(SATTH-THETAR)*PARA1*(-PSI2(J))**(PARB1-1.0)
            ACAP(J)=ACAP(J)/(PARA1+(-PSI2(J))**PARB1)**2.0
          ELSE
            ACON(J)=SATK*(PARA2/(PARA2+((-PSI2(J))**PARB2)))**PARN
            ACAP(J)=PARB2*(SATTH-THETAR)*PARA2*(-PSI2(J))**(PARB2-1.0)
            ACAP(J)=ACAP(J)/(PARA2+(-PSI2(J))**PARB2)**2.0
          ENDIF
  50    CONTINUE
C
C     Set up the RHS for the corrector.
C
        DO 60 J=M1,M
          CONU2(J)=(ACON(J+1)+ACON(J))/2.0
          CONL2(J)=(ACON(J-1)+ACON(J))/2.0
```

```
      A(J)=CONL2(J)
      B(J)=-CONU2(J)-CONL2(J)-(2.0*ACAP(J)*DELZ**2/DELT)
      C(J)=CONU2(J)
      D1=CONU1(J)*(PSI1(J+1)-PSI1(J)+DELZ)
      D2=CONL1(J)*(PSI1(J)-PSI1(J-1)+DELZ)
      D3=2.*DELZ**2*ACAP(J)*PSI1(J)/DELT
      RHS(J)=-D3-D1+D2-DELZ*(CONU2(J)-CONL2(J))
   60 CONTINUE
      RHS(M1)=RHS(M1)-PSI2(M1-1)*CONL2(M1)
      CONL2(MM)=(ACON(MM)+ACON(M))/2.0
      A(MM)=CONL2(MM)
      B(MM)=-CONL2(MM)-(2.0*ACAP(MM)*DELZ**2/DELT)
      D1=-2.0*ACAP(MM)*PSI1(MM)*DELZ**2/DELT
      D2=DELZ*(-2.0*R+CONL2(MM)+CONL1(MM))
      D3=CONL1(MM)*(PSI1(MM)-PSI1(M))
      RHS(MM)=D1+D2+D3
C
      CALL TRIDIA (M1,M2,M,MM)
C
C     Determine the new array of moisture contents, from the moisture-
C     tension characteristic curve.
C
      DO 70 J=M1,MM
        TPSI1(J)=PSI2(J)
   70 CONTINUE
      DO 80 J=M1,MM
        IF(TPSI1(J).GE.0.0) THEN
          THETA2(J)=SATTH
        ELSEIF (TPSI1(J).GE.XPT) THEN
          THETA2(J)=(SATTH-THETAR)*PARA1/(PARA1+((-TPSI1(J))**PARB1))
     1    +THETAR
        ELSE
          THETA2(J)=(SATTH-THETAR)*PARA2/(PARA2+((-TPSI1(J))**PARB2))
     1    +THETAR
        ENDIF
   80 CONTINUE
C
C     Calculate the change in moisture content.
C
      STOR=0.0
      DO 90 J=M1,MM
        DIFF=THETA2(J)-THETA1(J)
        PSTOR=DELZ*DIFF
        STOR=STOR+PSTOR
   90 CONTINUE
      STOR=STOR/DELT
      SMQ=R-STOR
C
C     Determine the minimum moisture content.
C
      TLEAST=THETA2(M1)
      DO 100 J=M2,MM
      I F(TLEAST.GE.THETA2(J)) TLEAST=THETA2(J)
  100 CONTINUE
C
C     Calculate specific yield.
C
      SPYD=SATTH-TLEAST
C
C     Calculate moisture balance.
C
      TSTOR=0.0
      TR=R*TIME
      DO 110 J=M1,MM
        DIFF=THETA2(J)-THETAI(J)
        PSTOR=DIFF*DELZ
        TSTOR=TSTOR+PSTOR
  110 CONTINUE
C
      DO 120 J=M1,MM
        PSI1(J)=TPSI1(J)
  120 CONTINUE
```

```
C
C     Keep track of total rate of drainage.
C
        TSMQ=TSMQ+SMQ
C
C     At printout iterations, determine average rate of drainage,
C     print information.
C
        IF(KOUNT.NE.KPNT) GO TO 18
          ASMQ=TSMQ/KPNT
          TDAYS=TIME/(24.0*3600.0)
C         WRITE (6,606)
          DO 125 J=M1,MM
             WRITE(6,621) J,TDAYS,THETA2(J)
 125      CONTINUE
          WRITE  (6,606)
          WRITE  (6,611)
          WRITE  (6,604)  STOR
          WRITE  (6,612)
          WRITE  (6,604)   SMQ
          WRITE  (6,617)
          WRITE  (6,604)  TSMQ
          WRITE  (6,619)
          WRITE  (6,604)  ASMQ
          WRITE  (6,616)
          WRITE  (6,603)  SPYD
          WRITE  (6,606)
          WRITE  (6,625)
          WRITE  (6,603)  TR
          WRITE  (6,626)
          WRITE  (6,603)  TSTOR
          WRITE  (6,606)
          TSMQ=0.0
          KOUNT=0
 18     KOUNT=KOUNT+1
 20   CONTINUE
      STOP
      END
C
C*******************************************************************
C
      SUBROUTINE TRIDIA (N1,N2,N,NN)
C
C*******************************************************************
C
        COMMON A,B,C,F,X,Z,ALPHA,BETA,DELZ,THETAI,
      1SATK,SATTH
        DIMENSION B(100),F(100),X(100)
        DIMENSION A(100),C(100)
        DIMENSION Z(100),ALPHA(100),BETA(100),THETAI(100)
C
        ALPHA(N1)=B(N1)
        BETA(N1)=C(N1)/ALPHA(N1)
        DO 130 I=N2,N
          ALPHA(I)=B(I)-A(I)*BETA(I-1)
          BETA(I)=C(I)/ALPHA(I)
 130    CONTINUE
        ALPHA(NN)=B(NN)-A(NN)*BETA(N)
        Z(N1)=F(N1)/ALPHA(N1)
        DO 140 I=N2,NN
          Z(I)=(F(I)-A(I)*Z(I-1))/ALPHA(I)
 140    CONTINUE
        X(NN)=Z(NN)
        NU=NN-N1
        DO 150 I=1,NU
          J=NN-I
          X(J)=Z(J)-BETA(J)*X(J+1)
 150    CONTINUE
        RETURN
        END
```

APPENDIX B. Data and partial output files

Data file A. Instantaneous profile test.

```
      51
       2
       2
0.003500     0.000000
       0          360
           60.0
           10.0
    1080
      60
             0.07
             0.385
             0.02
   306.5        0.984    89463.00       2.858         5.0
          -20.7
  -10.00       -20.00      -30.00      -40.00      -50.00      -60.00      -70.00      -80.00
  -90.00       -91.20      -91.20      -91.20      -91.20      -91.20      -91.20      -91.20
  -91.20       -91.20      -91.20      -91.20      -91.20      -91.20      -91.20      -91.20
  -91.20       -91.20      -91.20      -91.20      -91.20      -91.20      -91.20      -91.20
  -91.20       -91.20      -91.20      -91.20      -91.20      -91.20      -91.20      -91.20
  -91.20       -91.20      -91.20      -91.20      -91.20      -91.20      -91.20      -91.20
  -91.20       -91.20
```

Data file B. Fall rainstorms (51-day) simulation.

```
      51
       2
      30
0.000000     0.000350  0.000000    0.000036    0.000000    0.000069    0.000000    0.000036
0.000000     0.000140  0.000000    0.000036    0.000000    0.000140    0.000000    0.000028
0.000000     0.000039  0.000000    0.000011    0.000000    0.000053    0.000000    0.000036
0.000000     0.000053  0.000000    0.000058    0.000000    0.000092
       0           72          76         408         416         844         848         984
     992         1140        1144        1232        1240        1400        1440        1580
    1600         2500        2592        2892        2916        3744        3832        4244
    4312         4548        4584        4656        4704        4860
          900.0
           10.0
    4896
      96
             0.07
             0.385
             0.02
   306.5        0.984    89463.00       2.858         5.0
          -20.7
  -10.00       -20.00      -30.00      -40.00      -49.98      -59.94      -69.77      -79.16
  -87.12       -91.95      -93.86      -94.50      -94.82      -95.09      -95.29      -95.55
  -95.82       -96.02      -96.30      -96.57      -96.85      -97.13      -97.48      -97.76
  -98.12       -98.49      -98.86      -99.23      -99.60     -100.06     -100.45     -100.99
 -101.47      -102.03     -102.53     -103.19     -103.87     -104.57     -105.28     -106.19
 -107.12      -108.08     -109.27     -110.50     -112.00     -113.79     -115.79     -118.44
 -122.02      -127.30
```

APPENDIX B *continued*

Partial output file from Data file A.

```
                  The time step is (sec)
                    60.0000000000
  The infiltr. rates and corresponding iters. are
       0.003500          0.000000
              0                360

                  Nodal spacing is (cm)
    10.0000000000

       SATK (cm/sec), SATTH, THETAR are
   0.070000 0.385000 0.020000
       Brutsaert parameters A1, B1, A2, B2, N
       306.50000          0.98400     89463.00000          2.85800
        5.00000
  NODE  TIME(days)      THETA
            Moisture contents
          2         0.0000          0.3739
          3         0.0000          0.3636
          .
          .
         50         0.0000          0.0868
         51         0.0000          0.0868
          2         0.0417          0.3739
          3         0.0417          0.3636
          .
          .
         50         0.0417          0.2205
         51         0.0417          0.2205

          The rate of change of storage is
    0.3496942343E-02
  Rate of drainage out of the column (cm/sec)
    0.3057764843E-05
          Cumulative rate of drainage (cm/sec)
    0.2868131269E-03
          Average rate of drainage (cm/sec)
    0.4780218660E-05
          Specific yield
    0.2982364893

  TR (Total infiltration)
          12.6000003815
  TSTOR (Total storage change)
          12.5827913284
          .
          .
          .
```

APPENDIX C. Determining Brutsaert's parameters *A, B,* and *N*

Finding parameters *A* and *B*

Let

$$U = \frac{A}{[A + (-\psi)^B]} = \frac{(\theta - \theta_r)}{(\theta_0 - \theta_r)} \tag{C1}$$

(see equation 10). Plot

$$\frac{(\theta_0 - \theta_r)}{(\theta - \theta_r)} - 1 \tag{C2}$$

against $-\psi$ on log-log paper and draw the best straight line. Then,

$$\log[\frac{(\theta_0 - \theta_r)}{(\theta - \theta_r)} - 1] = \log[\frac{A + (-\psi)^B}{A} - 1] = \log\frac{(-\psi)^B}{A} = B\log(-\psi) + \log(1/A). \tag{C3}$$

Equation C3 is an equation for a straight line with slope equal to parameter B and intercept equal to log (1/A).

The functional relationship between log $(1/U - 1)$ and log $(-\psi)$ is shown in figure C1. Rather than approximate the curve by a poorly fitting straight line, we split the line into two segments, each of which is fitted by a straight line using linear regression. The resulting parameters are

$$A1 = 306.5$$
$$B1 = 0.98$$
$$A2 = 89{,}463$$
$$B2 = 2.858.$$

The recreated characteristic curve based on the fitted parameters is shown in figure 10d, with the constructed curve based on data shown in figure 10c.

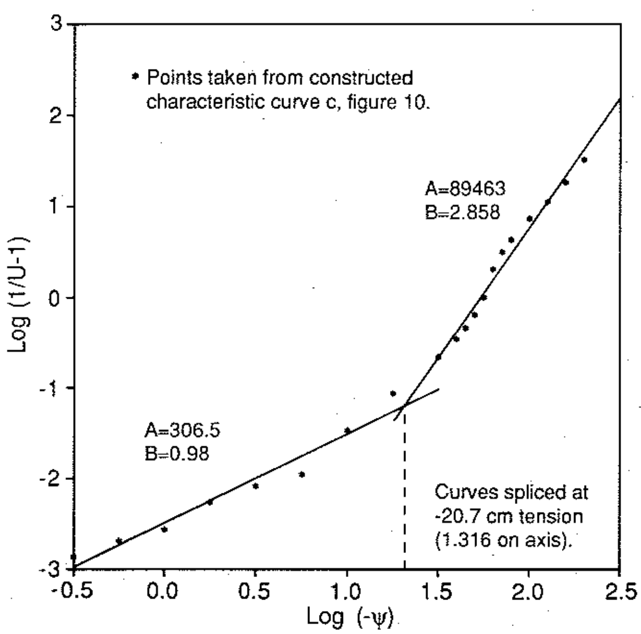

Figure C1. Functional relationship between log$(1/U - 1)$ and log$(-\psi)$ used to determine Brutsaert's parameters A and B. In this study the curve was treated as two segments, fitted separately, resulting in two sets of parameters. For tensions greater than -20.7 cm, $A2$ = 89,463 and $B2$ = 2.858. For wetter conditions, $A1$= 306.5 and $B1$ = 0.98. The slope of each segment is equal to B, and the intercept is equal to log(1/A).

Finding parameter N

The objective in this step is to find N such that the empirical function with A and B just derived fits the observed data well. The observed data are shown in figure C2. Because the $\theta(\psi)$ curve was spliced from two segments, the $K(\psi)$ curve will also be spliced at the same ψ value. The plot for N=5 is shown with the data for comparison. Although it is difficult to judge the fit of the curve in the range of tensions $0 < -\psi < 40$ cm, published $K(\psi)$ curves (Stephens and Knowlton, 1986; Denning and others, 1974) indicate that the shape of the curve is reasonable.

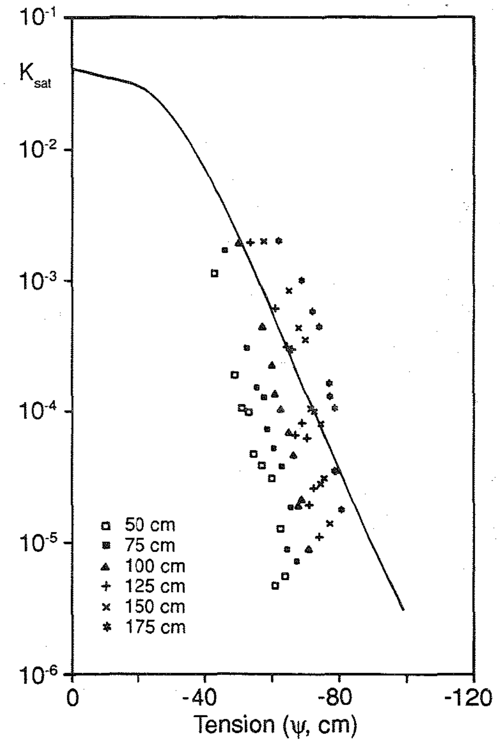

Figure C2. Measured (symbols) and fitted (solid curve) tension versus hydraulic conductivity. The fitted curve is constructed using Brutsaert's (1966) equation, with parameters $A1$ = 306.5; $B1$ = 0.98; $A2$ = 89,463; $B2$ = 2.858; and N = 5. Curve is spliced at a tension of -20.7 cm. The saturated hydraulic conductivity is 0.04 cm/sec.

University of Wisconsin—Extension
UWEX
GNHS
WISCONSIN GEOLOGICAL
and NATURAL HISTORY SURVEY

Cover: *Example of instrumentation and analysis for monitoring movement of water through the unsaturated zone in central Wisconsin. Left: Field instrumentation. Right: Measured and model-simulated moisture profiles at the same site.*

ISSN: 0512-0640